Available online at www.sciencedirect.com
SCIENCE DIRECT®
Journal of Computational Physics 206 (2005) 122–149
JOURNAL OF COMPUTATIONAL PHYSICS
www.elsevier.com/locate/jcp

An evolution Galerkin scheme for the shallow water magnetohydrodynamic equations in two space dimensions

Tim Kröger [a], Mária Lukáčová-Medvid'ová [b,*]

[a] Division of Numerical Mathematics IGPM, RWTH Aachen, Germany
[b] AB Mathematik, Technische Universität Hamburg-Harburg, Schwarzenbergstrasse 95, 21079 Hamburg, Germany

Received 26 April 2004; received in revised form 1 November 2004; accepted 24 November 2004
Available online 25 January 2005

Abstract

In this paper we propose a new finite volume evolution Galerkin (FVEG) scheme for the shallow water magnetohydrodynamic (SMHD) equations. We apply the exact integral equations already used in our earlier publications to the SMHD system. Then, we approximate these integral equation in a general way which does not exploit any particular property of the SMHD equations and should thus be applicable to arbitrary systems of hyperbolic conservation laws in two space dimensions. In particular, we investigate more deeply the approximation of the spatial derivatives which appear in the integral equations. The divergence free condition is satisfied discretely, i.e. at each vertex. First numerical results confirm reliability of the numerical scheme.

MSC: 76W05; 35L65; 65M06; 35L45; 35L67; 65M25
Keywords: Genuinely multidimensional schemes; Hyperbolic systems; Shallow water magnetohydrodynamic equations; Finite volume methods; Evolution Galerkin schemes

1. Introduction

We consider a system of hyperbolic conservation laws

$$\partial_t \boldsymbol{U} + \nabla_{\underline{x}} \cdot \underline{\boldsymbol{F}}(\boldsymbol{U}) = \boldsymbol{0}.$$

We use here the notation of the first author's dissertation [14], in which underlined symbols denote *row* vectors with d components and boldfaced symbols denote *column* vectors with m components. The double underlined symbols, that will be used later, denote row vectors with m components.

* Corresponding author. Tel.: +49 40 428 78 3670; fax: +49 40 428 78 2696.
E-mail address: lukacova@tu-harburg.de (M. Lukáčová-Medvid'ová).

0021-9991/$ - see front matter © 2005 Elsevier Inc. All rights reserved.
doi:10.1016/j.jcp.2004.11.031

Most classical numerical schemes for such systems are based on solving one-dimensional Riemann problems across the interfaces of a structured or unstructured mesh. The roots of this idea go back to Godunov [10], who invented the prototype of these schemes for one-dimensional systems.

However, there is an ongoing discussion, initiated by Roe [30], whether schemes which are based on solving one-dimensional Riemann problems can reflect all multidimensional effects occurring in multidimensional systems. In the literature we can find several genuinely multidimensional numerical schemes, which purposely dispensed with Riemann solvers, see e.g. [7,8,25,17,3].

In this paper, we will deal with the evolution Galerkin (EG) schemes, which also belong to this class of multidimensional Riemann solver free approaches. The main idea of these schemes is to evolve the solution along the bicharacteristic curves forming the Mach cone and then project it into the approximation space. Exact evolution of the solution in time is represented by the integral equations for a linear(ized) system, i.e. a solution representation involving integrals over intermediate time levels. In order to use this integral equations numerically, integrals are approximated by suitable numerical quadratures yielding the so-called approximate evolution operators. A paper due to Butler [4] can be considered to be the first contribution to the EG approach. This operator was later stated in a general way by Ostkamp [26,27], who also showed that there is a certain connection between the EG approach and Fey's [7,8] Method of Transport.

In the last years, Lukáčová, Morton et al. [19–22] constructed several EG schemes for the wave equation system, the shallow water equations, and the Euler equations, where they soon embedded the evolution operators into a finite volume framework, obtaining the so-called finite volume evolution Galerkin (FVEG) schemes. Extensive experimental treatment confirms that the EG and FVEG schemes approximate correctly complex multidimensional structures of solutions, e.g. circular expansion wave, oblique shocks, etc. Numerical comparisons with other well-known schemes illustrate high global accuracy of the FVEG schemes. For example the second order FVEG method is six times more accurate than the Lax–Wendroff scheme as well as the LeVeque wave propagation algorithm for linear hyperbolic systems, whereas the computational costs are comparable with the LeVeque scheme, see [20].

On the other hand, Kröger et al. [15,14] developed a framework of the so-called state decompositions, in which they examined the connection between the EG approach and the Method of Transport more deeply and managed to clarify an important difference between these approaches. At the same time, this framework offers the possibility to consider the EG approach from a different point of view.

In the current paper, we introduce an FVEG scheme for the shallow water magnetohydrodynamic (SMHD) equations. These equations were (to our knowledge) first proposed by Gilman [9] as an approximation to the ideal MHD equations in the situation of a free-surface, shallow, and electrically conducting fluid that has constant density and is in magnetohydrostatic balance in the vertical direction.

There are two main difficulties for the numerical treatment of the full MHD equations:

- The magnetic field should be kept divergence-free in any time.
- The numerical update should produce fully multidimensional as well as non-oscillatory solutions near discontinuities.

Since the full system of the MHD equations has a complicated eigenstructure, it is desirable to have a simpler model system that retains both main difficulties but at the same time has a simpler eigenstructure. The SMHD system not only serves as a simplified mathematical model, but it has its own physical applicability used in the description of the solar tachocline, i.e. a thin layer of the solar radius that separates the convective zone from the radiative zone in stars, cf. [6,9].

As far as we know, this is the first FVEG approach for these equations. A second new property of the scheme is that it is mainly a black-box approach: while former approximate evolution operators, used in the FVEG schemes, were mostly specially designed for the individual system, the current scheme does not exploit any particular property of the SMHD equations. Therefore, the scheme should be applicable to

any system of hyperbolic conservation laws in two space dimensions without major changes. [1] In general it is also possible to apply the scheme to the ideal MHD equations (for two-dimensional problems), but further considerations due to a more complicated structure of the full MHD equations are necessary in order to obtain an efficient method. In this paper we content ourselves with the study of a model SMHD system. The first numerical experiments presented here show that the scheme gives good numerical results and indicate the reliability of the FVEG scheme for the modelling of the SMHD system.

The outline of this paper is as follows: in Section 2, we introduce briefly the SMHD equations and discuss a variant of them which is no longer conservative, but simpler and will in particular have a simpler hyperbolic structure. Next, in Section 3, we state the integral equations in an abstract, but compact, form which is also used in the works of Kröger et al. [15,14]. A brief description of the FVEG schemes follows in Section 4. We explain in detail how our new scheme works in Section 5. This mainly consists of a description of the used approximation techniques in the evolution operator as well as in the finite volume update formula. A main focus is set on the approximation of the spatial derivatives which occur in the evolution operator, since all the other approximations are performed using standard techniques. To summarize the presentation of the FVEG scheme for the SMHD equations we finish the Section 5 with the presentation of the numerical algorithm. Section 6 contains a couple of numerical experiments. Finally, in Section 7, we derive some conclusions.

2. The SMHD equations

2.1. The SMHD system of hyperbolic conservation laws

The SMHD equations were, as far as we know, first proposed by Gilman [9]. Afterwards, DeSterck [6] and Rossmanith [31], among others, worked on these equations. The SMHD equations can be derived from the ideal MHD equations. They model the dynamics of a constant density, shallow, and electrically conducting fluid that is hydrostatically balanced in the vertical direction. A detailed derivation is given by Rossmanith [31]. The result is a system of $m = 5$ equations in $d = 2$ space dimensions, which is given by

$$\partial_t \tilde{\boldsymbol{U}} + \nabla_{\underline{x}} \cdot \underline{\boldsymbol{F}}(\tilde{\boldsymbol{U}}) = \boldsymbol{C}(\tilde{\boldsymbol{U}}), \tag{2.1}$$

where

$$\tilde{\boldsymbol{U}} = \begin{pmatrix} h \\ h\underline{u}^{\mathrm{T}} \\ h\underline{B}^{\mathrm{T}} \end{pmatrix}, \quad \underline{\boldsymbol{F}}(\tilde{\boldsymbol{U}}) = \begin{pmatrix} h\underline{u} \\ h\underline{u}^{\mathrm{T}}\underline{u} - h\underline{B}^{\mathrm{T}}\underline{B} + \frac{1}{2}gh^2\underline{\mathbf{1}} \\ h\underline{B}^{\mathrm{T}}\underline{u} - h\underline{u}^{\mathrm{T}}\underline{B} \end{pmatrix}, \quad \boldsymbol{C}(\tilde{\boldsymbol{U}}) = \begin{pmatrix} 0 \\ -gh\nabla b \\ \underline{0}^{\mathrm{T}} \end{pmatrix}. \tag{2.2}$$

More precisely, we can rewrite (2.1) as

$$\partial_t \tilde{\boldsymbol{U}} + \partial_{x_1} \boldsymbol{F}_1(\tilde{\boldsymbol{U}}) + \partial_{x_2} \boldsymbol{F}_2(\tilde{\boldsymbol{U}}) = \boldsymbol{C}(\tilde{\boldsymbol{U}}) \tag{2.3}$$

with

$$\underline{\boldsymbol{F}}(\tilde{\boldsymbol{U}}) = \big(\boldsymbol{F}_1(\tilde{\boldsymbol{U}}), \boldsymbol{F}_2(\tilde{\boldsymbol{U}})\big).$$

The system (2.1) or (2.3), is moreover accompanied with the intrinsic constraint

$$\nabla \cdot (h\underline{B}) = 0. \tag{2.4}$$

[1] However, we exploit essentially the fact that the physical space is two-dimensional, i.e. $d = 2$.

Recall that the notation is adopted from [14]. Further, $g > 0$ is the gravitational constant, and $b = b(\underline{x})$ describes the bottom topography. In the current paper, we restrict ourselves to the case of a flat bottom, i.e. $b = \text{const.}$, so that the system is homogeneous. We deal with the numerical approximation of the time-dependent system (2.1) and derive the approximation of the divergence constraint (2.4), which is satisfied by a numerical solution. Note that this constraint is also exploited in the reformulation of the system (2.1) which is realized in Section 2.2.

These equations can be rewritten in terms of the primitive variables $\boldsymbol{U} = (h, \underline{u}, \underline{B})^{\mathrm{T}}$, yielding

$$\partial_t h + \underline{u}\nabla h + h\nabla^{\mathrm{T}}\underline{u}^{\mathrm{T}} = 0,$$

$$\partial_t \underline{u} + g\nabla^{\mathrm{T}} h - \frac{1}{h}\underline{B}\nabla h\underline{B} + \underline{u}\nabla\underline{u} - \nabla^{\mathrm{T}}\underline{B}^{\mathrm{T}}\underline{B} - \underline{B}\nabla\underline{B} = \underline{0},$$

$$\partial_t \underline{B} - \frac{1}{h}\underline{B}\nabla h\underline{u} - \underline{B}\nabla\underline{u} + \underline{u}\nabla\underline{B} - \nabla^{\mathrm{T}}\underline{B}^{\mathrm{T}}\underline{u} = \underline{0},$$

where the symbol ∇ always denotes a *column* vector of derivatives. This can be written in the form

$$\partial_t \boldsymbol{U} + \sum_{s=1}^{2} \tilde{\underline{\underline{A}}}_s(\boldsymbol{U})\partial_{x_s}\boldsymbol{U} = \boldsymbol{0}, \tag{2.5}$$

where

$$\tilde{\underline{\underline{A}}}_1 n_1 + \tilde{\underline{\underline{A}}}_2 n_2 = \begin{pmatrix} \underline{u}\cdot\underline{n} & h\underline{n} & \underline{0} \\ g\underline{n}^{\mathrm{T}} - \frac{1}{h}(\underline{B}\cdot\underline{n})\underline{B}^{\mathrm{T}} & (\underline{u}\cdot\underline{n})\underline{\mathbf{1}} & -\underline{B}^{\mathrm{T}}\underline{n} - (\underline{B}\cdot\underline{n})\underline{\mathbf{1}} \\ -\frac{1}{h}(\underline{B}\cdot\underline{n})\underline{u}^{\mathrm{T}} & -(\underline{B}\cdot\underline{n})\underline{\mathbf{1}} & (\underline{u}\cdot\underline{n})\underline{\mathbf{1}} - \underline{u}^{\mathrm{T}}\underline{n} \end{pmatrix},$$

$\underline{\mathbf{1}}$ denotes a 2×2 unit matrix, and $\underline{n} = (n_1, n_2)$ is an arbitrary non-zero vector in $\mathbb{R}^2$. Of course, the system (2.5) will have a different solutions than (2.1) in the case of discontinuities, but this does not matter since we will use the system (2.1), that is written in the conservative form, in the finite volume update. Nevertheless, (2.5) is suitable to examine the hyperbolic structure of the system and derive the approximate evolution operator, cf. Section 5.

2.2. A Powell-like form for the SMHD equations

The SMHD equations have got the intrinsic constraint $\nabla\cdot(h\underline{B}) = 0$. This means, that the exact solution will satisfy this constraint for all time if it holds for the initial data. This can be seen by computing $\partial_t(\nabla\cdot(h\underline{B}))$. In physically relevant problems, the initial data will always satisfy this constraint.

This is a similarity to the MHD equations, in which $\nabla\cdot\underline{B}$ remains zero for all time. In 1972, Godunov [11] exploited this property by adding certain multiples of $\nabla\cdot\underline{B}$ to each equation – thus not changing the exact solutions in the physically relevant situation – in such a way that the resulting equations have nicer properties. Later, Powell [28] used this form for a numerical scheme. This alternative form of the MHD equations, which we will call 'Powell's form', was also favored by Brackbill and Barnes [1] and by Kröger [14]. Since in particular the hyperbolic structure of the system becomes much simpler for Powell's form, we find it desirable to construct a Powell-like form for the SMHD equations as well. Here we may add a multiple of

$$\nabla\cdot(h\underline{B}) = \nabla^{\mathrm{T}} h\underline{B}^{\mathrm{T}} + h\nabla^{\mathrm{T}}\underline{B}^{\mathrm{T}} = \underline{B}\nabla h + h\nabla^{\mathrm{T}}\underline{B}^{\mathrm{T}}$$

rather than $\nabla\cdot\underline{B}$ to each equation. By this, we can easily get the simpler system

$$\partial_t h + \underline{u}\nabla h + h\nabla^{\mathrm{T}}\underline{u}^{\mathrm{T}} = 0,$$

$$\partial_t \underline{u} + g\nabla^{\mathrm{T}} h + \underline{u}\nabla\underline{u} - \underline{B}\nabla\underline{B} = \underline{0},$$

$$\partial_t \underline{B} - \underline{B}\nabla\underline{u} + \underline{u}\nabla\underline{B} = \underline{0}.$$

If we write it in the compact vector form

$$\partial_t \boldsymbol{U} + \sum_{s=1}^{2} \underline{\underline{\boldsymbol{A}}}_s(\boldsymbol{U})\partial_{x_s}\boldsymbol{U} = \boldsymbol{0}, \tag{2.6}$$

we get

$$\underline{\underline{\boldsymbol{A}}}_1 n_1 + \underline{\underline{\boldsymbol{A}}}_2 n_2 = \begin{pmatrix} \underline{u}\cdot\underline{n} & h\underline{n} & \underline{0} \\ g\underline{n}^{\mathrm{T}} & (\underline{u}\cdot\underline{n})\underline{\mathbf{1}} & -(\underline{B}\cdot\underline{n})\underline{\mathbf{1}} \\ \underline{0} & -(\underline{B}\cdot\underline{n})\underline{\mathbf{1}} & (\underline{u}\cdot\underline{n})\underline{\mathbf{1}} \end{pmatrix}. \tag{2.7}$$

The system (2.6) is a starting point for developing a suitable approximation of the integral equations, which is used in order to predict fluxes on cell interfaces in the FVEG schemes, cf. (4.2).

3. Integral equations

3.1. Overview for general systems

For a general *linear* hyperbolic system

$$\partial_t \boldsymbol{U} + \sum_{s=1}^{d} \underline{\underline{\boldsymbol{A}}}_s \partial_{x_s}\boldsymbol{U} = \boldsymbol{0}, \tag{3.1}$$

one has the exact integral equations, which were first proposed by Ostkamp [26] and later extensively used by Lukáčová et al. [19–22]. They can be derived using the general characteristic theory for linear(ized) hyperbolic systems and written in the compact, but abstract, form

$$\begin{aligned} \boldsymbol{U}(\underline{x}, t_{n+1}) = \frac{1}{|S^{d-1}|}\sum_{k=1}^{m}\Bigg(&\int_{S^{d-1}} \boldsymbol{r}^k_{\underline{n}}\underline{\underline{l}}^k_{\underline{n}}\boldsymbol{U}(\underline{x} - \Delta t\nabla_{\underline{n}}\lambda^k_{\underline{n}}, t_n)\mathrm{d}\underline{n} \\ &+ \int_{t_n}^{t_{n+1}}\int_{S^{d-1}} \boldsymbol{r}^k_{\underline{n}}\underline{\underline{l}}^k_{\underline{n}}\sum_{s=1}^{d}(\partial_{n_s}\lambda^k_{\underline{n}}\cdot\underline{\underline{\mathbf{1}}} - \underline{\underline{\boldsymbol{A}}}_s)\partial_{x_s}\boldsymbol{U}(\underline{x} + (\tau - t_{n+1})\nabla_{\underline{n}}\lambda^k_{\underline{n}}, \tau)\mathrm{d}\underline{n}\,\mathrm{d}\tau\Bigg). \end{aligned} \tag{3.2}$$

Here, $\boldsymbol{r}^k_{\underline{n}}$, $\underline{\underline{l}}^k_{\underline{n}}$ and $\lambda^k_{\underline{n}}$ are the right eigenvectors, left eigenvectors, and the eigenvalues of the matrix pencil $\sum_{s=1}^{d}\underline{\underline{\boldsymbol{A}}}_s n_s$, respectively. We assume that the left and right eigenvectors are normalized such that $\underline{\underline{l}}^k_{\underline{n}}\boldsymbol{r}^k_{\underline{n}} = 1$. Note that $\nabla_{\underline{n}}\lambda^k_{\underline{n}}$ are the ray velocities arising from the multidimensional characteristic theory, compare [5,13,29], or [14]. It can be shown that

$$\partial_{n_s}\lambda^k_{\underline{n}} = \underline{\underline{l}}^k_{\underline{n}}\underline{\underline{\boldsymbol{A}}}_s\boldsymbol{r}^k_{\underline{n}}, \quad s = 1,\ldots,d. \tag{3.3}$$

Thus, there is the alternative representation $(\underline{\underline{l}}^k_{\underline{n}}\underline{\underline{\boldsymbol{A}}}_1\boldsymbol{r}^k_{\underline{n}}, \ldots, \underline{\underline{l}}^k_{\underline{n}}\underline{\underline{\boldsymbol{A}}}_d\boldsymbol{r}^k_{\underline{n}})$ for the ray velocities $\nabla_{\underline{n}}\lambda^k_{\underline{n}}$.

We should point out that for a non-linear system, there is also a fully non-linear form of (3.3), see [14]. However, this leads to a more complex formula. Hence, for practical applications, it seems to be easiest to apply (3.2) to a linearized system. In other words, one first freezes the matrices $\underline{\underline{\boldsymbol{A}}}_s$ (and therefore, also the eigenvectors and eigenvalues) at a given state $\hat{\boldsymbol{U}}$, and then applies (3.2). In this paper, we always denote by $\hat{\boldsymbol{U}}$ the linearization state, whereas $\check{\boldsymbol{U}}$ denotes the solution of the linearized system. With this notation, the linearized system reads

$$\partial_t \check{\boldsymbol{U}} + \sum_{s=1}^{d} \underline{\underline{\boldsymbol{A}}}_s(\hat{\boldsymbol{U}})\partial_{x_s}\check{\boldsymbol{U}} = \boldsymbol{0}.$$

Notations $\hat{}$ and $\check{}$ are also used for any conservative or primitive variables with the obvious meanings. However, for a better readability, we leave out both notations whenever there is no danger of confusion.

3.2. Application to the SMHD equations

Instead of deriving the respective integral representations for the primitive components h, $\underline{u}$, and $\underline{B}$ arising from the general operator (3.2) we content ourselves with giving suitable representations for the ingredients appearing in the general formula. We do this for the Powell-like form (2.7) derived in Section 2.2. A representation for the matrices $\underline{\underline{\boldsymbol{A}}}_s$ has already been given in (2.7) The eigenvalues read

$$\lambda^1_{\underline{n}} = \underline{u}\cdot\underline{n} + \underline{B}\cdot\underline{n}, \quad \lambda^2_{\underline{n}} = \underline{u}\cdot\underline{n} - \underline{B}\cdot\underline{n}, \quad \lambda^3_{\underline{n}} = \underline{u}\cdot\underline{n} + W, \quad \lambda^4_{\underline{n}} = \underline{u}\cdot\underline{n} - W, \quad \lambda^5_{\underline{n}} = \underline{u}\cdot\underline{n},$$

where we used the abbreviation

$$W = \sqrt{(\underline{B}\cdot\underline{n})^2 + gh|\underline{n}|^2}.$$

We call the first two wave modes Alfvén waves, the third and the fourth ones are the magneto-gravity waves and the last mode, which propagates with the fluid speed, is called the non-physical mode in an analogy to the ideal MHD equations.

The corresponding right eigenvectors are

$$\boldsymbol{r}^1_{\underline{n}} = \frac{1}{2|\underline{n}|^2}\begin{pmatrix} 0 \\ -\underline{p}^{\mathrm{T}} \\ \underline{p}^{\mathrm{T}} \end{pmatrix}, \quad \boldsymbol{r}^2_{\underline{n}} = \frac{1}{2|\underline{n}|^2}\begin{pmatrix} 0 \\ \underline{p}^{\mathrm{T}} \\ \underline{p}^{\mathrm{T}} \end{pmatrix}, \quad \boldsymbol{r}^3_{\underline{n}} = \frac{1}{2|\underline{n}|^2 W^2}\begin{pmatrix} h|\underline{n}|^2 \\ \underline{n}^{\mathrm{T}} W \\ -\underline{n}^{\mathrm{T}}(\underline{B}\cdot\underline{n}) \end{pmatrix},$$

$$\boldsymbol{r}^4_{\underline{n}} = \frac{1}{2|\underline{n}|^2 W^2}\begin{pmatrix} h|\underline{n}|^2 \\ -\underline{n}^{\mathrm{T}} W \\ -\underline{n}^{\mathrm{T}}(\underline{B}\cdot\underline{n}) \end{pmatrix}, \quad \boldsymbol{r}^5_{\underline{n}} = \frac{1}{W^2}\begin{pmatrix} \underline{B}\cdot\underline{n} \\ \underline{0}^{\mathrm{T}} \\ \underline{n}^{\mathrm{T}} g \end{pmatrix},$$

and the left eigenvectors read

$$\underline{l}^1_{\underline{n}} = (0, -\underline{p}, \underline{p}), \quad \underline{l}^2_{\underline{n}} = (0, \underline{p}, \underline{p}), \quad \underline{l}^3_{\underline{n}} = \Big(g|\underline{n}|^2, \underline{n}W, -\underline{n}(\underline{B}\cdot\underline{n})\Big), \quad \underline{l}^4_{\underline{n}} = \Big(g|\underline{n}|^2, -\underline{n}W, -\underline{n}(\underline{B}\cdot\underline{n})\Big),$$
$$\underline{l}^5_{\underline{n}} = (\underline{B}\cdot\underline{n}, \underline{0}, \underline{n}h),$$

where for the given normal direction $\underline{n}$, we denote by $\underline{p}$ the transversal direction, which in the two-dimensional case is canonically (up to a factor ± 1) given by

$$\underline{p} = (-n_2, n_1).$$

Note that this becomes essentially different in three dimensions where, as a consequence of the Hedgehog theorem, there cannot be a canonical basis of the two-dimensional space of transversal directions.

Finally, we also give the following formulae for the ray velocities

$$\nabla_{\underline{n}}\lambda^1_{\underline{n}} = \underline{u} + \underline{B}, \quad \nabla_{\underline{n}}\lambda^2_{\underline{n}} = \underline{u} - \underline{B}, \quad \nabla_{\underline{n}}\lambda^3_{\underline{n}} = \underline{u} + \frac{\underline{B}(\underline{B}\cdot\underline{n}) + \underline{n}gh}{W}, \quad \nabla_{\underline{n}}\lambda^4_{\underline{n}} = \underline{u} - \frac{\underline{B}(\underline{B}\cdot\underline{n}) + \underline{n}gh}{W}, \quad \nabla_{\underline{n}}\lambda^5_{\underline{n}} = \underline{u}.$$

One main advantage of the SMHD equations over the MHD equations is that there are no case distinctions or singular cases in the evaluation of the hyperbolic structure. In fact, the given formulae for the

eigenvectors do not cause numerical problems in the evaluation as far as physically reasonable restrictions $g > 0$ and $h > 0$ hold. If $\underline{B} \cdot \underline{n} = 0$, i.e. the normal magnetic field vanishes, we get a triple eigenvalue $u \cdot \underline{n}$. Fig. 3.1 shows the shape of the wave fronts, the so-called Friedrichs diagrams, for a selection of linearization states.

Note that it can easily be seen that, up to shift, rotation, and scale operations, the shape of the wave fronts is completely defined by the scalar parameter $|\underline{B}|^2/gh$. The given selection of wave fronts is representative in the sense that it contains one example for each of the cases where the parameter $|\underline{B}|^2/gh$ is zero, positive but small, smaller than 1, exactly 1, larger than 1, and large but finite.

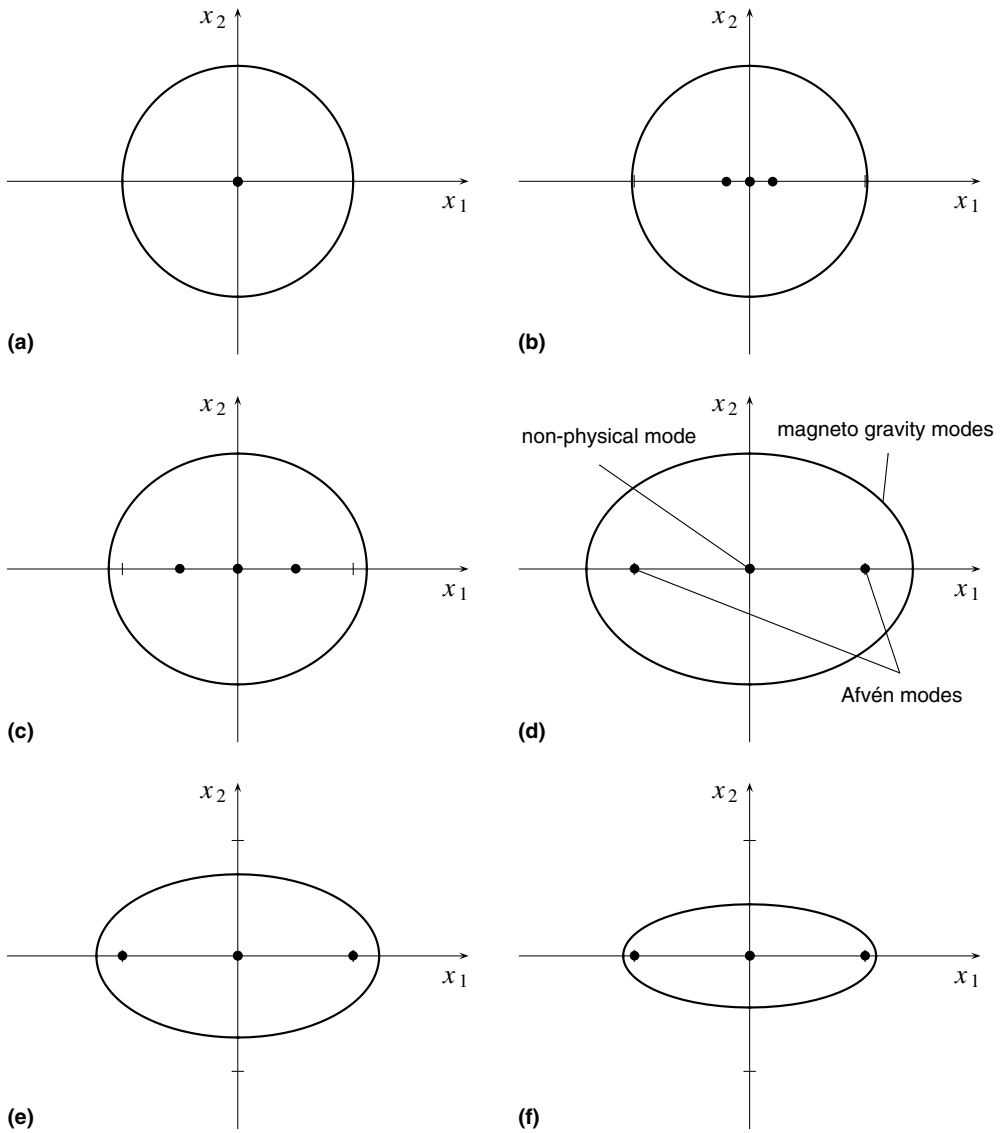

Fig. 3.1. Friedrichs diagrams for SMHD equations for $\underline{u} = \underline{0}$, $g = 1$, and (a) $h = 1$, $\underline{B} = (0, 0)$, (b) $h = 1$, $\underline{B} = (0.2, 0)$, (c) $h = 1$, $\underline{B} = (0.5, 0)$, (d) $h = 1$, $\underline{B} = (1, 0)$, (e) $h = 0.5$, $\underline{B} = (1, 0)$, (f) $h = 0.2$, $\underline{B} = (1, 0)$.

4. FVEG schemes

Consider an arbitrary system of hyperbolic conservation laws,

$$\partial_t \boldsymbol{U} + \partial_{x_1} \boldsymbol{F}_1(\boldsymbol{U}) + \partial_{x_2} \boldsymbol{F}_2(\boldsymbol{U}) = \boldsymbol{0}, \tag{4.1}$$

on a regular, cartesian, two-dimensional mesh, consisting of cells

$$K_{ij} = (x_{i-\frac{1}{2}}, x_{i+\frac{1}{2}}) \times (y_{j-\frac{1}{2}}, y_{j+\frac{1}{2}}),$$

where $x_{i\pm\frac{1}{2}} = (i \pm \frac{1}{2})\hbar$ and $y_{j\pm\frac{1}{2}} = (j \pm \frac{1}{2})\hbar$, $\hbar$ is a mesh step. If we integrate (4.1) in space over one cell K_{ij} and in time over the interval $[t_n, t_{n+1}]$ (where $t_n = n\Delta t$) and then apply the Gauss law, we get

$$\begin{aligned} \boldsymbol{U}_{ij}^{n+1} = \boldsymbol{U}_{ij}^{n} &- \frac{1}{|K_{ij}|} \int_{t_n}^{t_{n+1}} \int_{y_{j-\frac{1}{2}}}^{y_{j+\frac{1}{2}}} \Big(\boldsymbol{F}_1(\boldsymbol{U}(x_{i+\frac{1}{2}}, y, t)) - \boldsymbol{F}_1(\boldsymbol{U}(x_{i-\frac{1}{2}}, y, t)) \Big) \mathrm{d}y \, \mathrm{d}t \\ &- \frac{1}{|K_{ij}|} \int_{t_n}^{t_{n+1}} \int_{x_{i-\frac{1}{2}}}^{x_{i+\frac{1}{2}}} \Big(\boldsymbol{F}_2(\boldsymbol{U}(x, y_{j+\frac{1}{2}}, t)) - \boldsymbol{F}_2(\boldsymbol{U}(x, y_{j-\frac{1}{2}}, t)) \Big) \mathrm{d}x \, \mathrm{d}t, \end{aligned} \tag{4.2}$$

where

$$\boldsymbol{U}_{ij}^{n} = \frac{1}{|K_{ij}|} \int_{K_{ij}} \boldsymbol{U}(x, y, t_n) \mathrm{d}x \, \mathrm{d}y.$$

The idea of a finite volume evolution Galerkin (FVEG) scheme is to derive an update procedure for the cell averages $\boldsymbol{U}_{ij}^{n}$ by inserting the exact integral equations (3.2) into the finite volume update formula (4.2) in order to evaluate fluxes on cell interfaces. Then, suitable numerical approximation techniques are applied to everything in the resulting formula which cannot be evaluated exactly, see, e.g. [20,21] for more details.

The finite volume update formula (4.2) must be applied in conservative variables, while the approximate evolution operator will typically (but not necessarily) work with some primitive variables. In particular, for the SMHD equations, we will construct the approximate evolution operator to the Powell-like form in primitive variables (2.4). Also, note that the finite volume update formula is typically applied to the fully non-linear system (because in general, there will not be a reasonable global linearization state), whereas the evolution operator (3.2) requires a linearization. Therefore a suitable linearization state needs to be determined before each application of the evolution operator.

5. Approximation of the integral equations

In order to use the exact integral equation (3.2) numerically several approximations have to be made. This yields the so-called approximate evolution operator. More precisely, the following building blocks are necessary:

1. the recovery of a spatial function U constructed from the cell averages,
2. the time integration which occurs in the finite volume formulation,
3. the integration along cell interfaces occurring in the finite volume formulation,
4. the choice of the linearization state,
5. the integration over S^{d-1} in the integral equation (3.2),
6. the time integral in the second part of the integral equation (3.2), and
7. the evaluation of the spatial derivatives of U in the second part of the integral equation (3.2).

The items 1–6 will be realized with standard approximation techniques as described in the following subsection, whereas the last item has to be investigated carefully in order to obtain suitable results. This will be discussed in Section 5.2. In order to summarize the whole FVEG scheme we present in Section 5.3 the numerical algorithm.

5.1. The use of standard approximation techniques

In order to get a function defined on a computational domain Ω by means of a given family of cell averages, we use a conservative, piecewise bilinear recovery. More precisely, if we have given cell averages ψ_{ij} on a regular mesh with mesh size $\hbar$, we approximate the exact solution on the mesh cell K_{ij} by a bilinear function

$$\hat{\psi}(\underline{x})|_{K_{ij}} = \psi_{ij} + (x_1 - x_1^0)\psi_{ij}^1 + (x_2 - x_2^0)\psi_{ij}^2 + (x_1 - x_1^0)(x_2 - x_2^0)\psi_{ij}^{12},$$

where $\underline{x}^0$ is the center of K_{ij} and the coefficients ψ_{ij}^1, ψ_{ij}^2, and ψ_{ij}^{12}, which approximate derivatives, are given by

$$\psi_{ij}^1 = \frac{\psi_{i+1,j} - \psi_{ij}}{\hbar}\,\varphi\left(\frac{\psi_{ij} - \psi_{i-1,j}}{\psi_{i+1,j} - \psi_{ij}}\right),$$

$$\psi_{ij}^2 = \frac{\psi_{i,j+1} - \psi_{ij}}{\hbar}\,\varphi\left(\frac{\psi_{ij} - \psi_{i,j-1}}{\psi_{i,j+1} - \psi_{ij}}\right),$$

$$\psi_{ij}^{12} = \frac{\psi_{i+1,j+1} + \psi_{i-1,j-1} - 2\psi_{ij}}{\hbar^2}\,\varphi\left(\frac{2\psi_{ij} - \psi_{i+1,j-1} - \psi_{i-1,j+1}}{\psi_{i+1,j+1} + \psi_{i-1,j-1} - 2\psi_{ij}}\right).$$

Here, φ is a limiter function out of the class that was discussed by Sweby [32]. We have made positive experience with the monotonized centered limiter, also known as minmod-2, which is given by

$$\varphi(\theta) = \begin{cases} 0, & \theta \leqslant 0, \\ 2\theta, & 0 \leqslant \theta \leqslant \frac{1}{3}, \\ \frac{1}{2}(1+\theta), & \frac{1}{3} \leqslant \theta \leqslant 3, \\ 2, & 3 \leqslant \theta. \end{cases}$$

Recall that the idea of this limiter is to use unlimited central differences as long as they are contained in the so-called second-order TVD region, cf. [32]. This reconstruction is done for every component of the primitive variables.

For the integrals appearing in the finite volume formulation we have already made good experience with the midpoint rule in time and Simpson's rule along the cell interfaces for hydrodynamical problems, see [20]. Therefore, we use for the first three equations of the SMHD system, i.e. for the hydrodynamical part, Simpson's rule for the cell interface integrals. Further, we use the trapezoidal rule for the last two equations, i.e. the Maxwell equations. Such a flux discretization leads to the FVEG scheme that automatically satisfies a discrete version of the divergence condition (2.4), cf. also (6.1). Note that the finite volume update is always done in the conservative variables and for the conventional form (2.1) (in contrast to the Powell-like form) of the equations. This ensures that the overall scheme is conservative.

According to our quadrature rules along the cell interfaces, we need to apply the approximate evolution operator centered at the cell vertices as well as at the midpoints of the cell interfaces. For the linearization state we use averages of the four or two cells next to the point in which the operator is applied.

In [19–21], the second author constructed schemes in which the integrals over the sonic circle S^1 were evaluated exactly. Due to the complexity of the SMHD equations this seems no longer to be possible now. We have therefore decided to evaluate these integrals by suitable quadrature rules. Due to the periodicity, it is irrelevant whether the rectangle rule or the trapezoidal rule is used. As quadrature points, we chose the points $(\cos\theta_i, \sin\theta_i)$, where θ_i either takes the values

$$\frac{2\pi i}{n} \quad \text{or} \quad \frac{2\pi(i+\frac{1}{2})}{n},$$

where in both cases n is the number of quadrature points (which due to symmetry reasons should be a multiple of 4) and $i = 1, \ldots, n$. In the second version, we purposely avoid that θ_i becomes a multiple of $\pi/2$. In our numerical examples in Section 6, we have used the second variant with $n = 8$ or $n = 16$ points. We have experimented also with different number of integration points n, which were distributed always regularly due to the periodicity of integrands. Numerical results showed only marginal differences.

Finally, the time integral in the second part of the integral equations (3.2) was simply approximated by the rectangle rule. We should point out that in the recent work of Lukáčová et al. [20], a new approximation of time integrals along the Mach cone was proposed in such a way that any one-dimensional plane wave aligned with the grid is computed exactly. This approximate evolution operator was derived for the wave equation system, the shallow water equations, and the Euler equations and yields more stable and accurate FVEG schemes. Application of this idea for the SMHD equations should be investigated in future.

5.2. Evaluation of the spatial derivatives

It would be possible to take approximations to the spatial derivatives of $\boldsymbol{U}$ in (3.2) according to the slopes of the piecewise bilinear reconstruction. However, these might be very poor approximations. In particular, when a term involving these derivatives is integrated along a path which crosses a cell interface (which typically is the case), this approximation fails to include the necessary Dirac distribution for the discontinuity of the reconstructed $\boldsymbol{U}$.

For the wave equation system, the second author [19] found a possibility to transform the integral equations in such a way, that all spatial derivatives disappear. The procedure how to do this consisted of two essential ideas, one of which was applied to the single wave mode for which the wave front concentrates to a single point, and the other was applied to the remaining modes. This distinction between two types of wave modes is typical for the general ideas of the current subsection. In what follows, we distinguish between the so-called singular and non-singular wave modes; the more precise explanation will follow.

5.2.1. Non-singular wave modes

We first concentrate on the wave modes with non-singular wave fronts. For these modes, the so-called 'useful lemma' was used in [19] to transform the space integral in such a way that the spatial derivatives disappear, see [19, Lemma 2.1]. The main idea of this lemma is to recognize that the spatial derivatives of $\boldsymbol{U}$ in (3.2) are always derivatives in a direction tangential to the integration path. This

makes it possible to rewrite them as derivatives with respect to θ (where θ is the variable which parameterizes the path) and then to use integration by parts. This shifts the θ derivative to known terms (which originate from the hyperbolic structure of the system), so that the derivatives can be performed in advance.

Thus, the key point is just the fact that the direction of the spatial derivative is tangential to the integration path. We will now prove that this is true for arbitrary hyperbolic systems, so that there is always a generalization of this 'useful lemma' for the non-singular wave modes. However, as it turns out, before one can apply the integration by parts, it is necessary to divide by the length element of the integration path. For some wave modes, this length element may vanish. This is the reason why there is no such 'useful lemma' for those modes, which we call singular wave modes.

The essential expression to examine is

$$\underline{\underline{l}}_{\underline{n}}^{k} \sum_{s=1}^{d} (\partial_{n_s} \lambda_{\underline{n}}^{k} \cdot \underline{\underline{\mathbf{1}}} - \underline{\underline{\boldsymbol{A}}}_s) \partial_{x_s} \boldsymbol{U}, \tag{5.1}$$

compare (3.2), where $d = 2$. (In particular, the leading factor $\boldsymbol{r}_{\underline{n}}^{k}$ only makes a vector out of the scalar-valued expression in (5.1) but has got no influence on the direction of the derivative.) Precisely, (5.1) is a sum of directional derivatives of the m components of the vector $\boldsymbol{U}$. This derivative is evaluated at the point $\underline{x} + \sigma \nabla_{\underline{n}} \lambda_{\underline{n}}^{k}$, where $\sigma = \tau - t_{n+1}$. If we parameterize the integration path by θ, i.e. we set

$$\underline{n} = \underline{n}(\theta) = (\cos\theta, \sin\theta), \tag{5.2}$$

then our goal is to show that the direction of each of the directional derivatives in (5.1) is tangential to the derivative with respect to θ of the point at which (5.1) is evaluated, i.e. tangential to $\partial_\theta \nabla_{\underline{n}} \lambda_{\underline{n}(\theta)}^{k}$. But it follows from the characteristic theory that $\partial_\theta \nabla_{\underline{n}} \lambda_{\underline{n}(\theta)}^{k}$ is always orthogonal to $\underline{n}(\theta)$. This is because $\partial_\theta \nabla_{\underline{n}} \lambda_{\underline{n}(\theta)}^{k}$ is of course tangential to the wave front, whereas $\underline{n}(\theta)$ is known to be the normal direction, i.e. normal to the wave front (see also [14, end of Section 3.4]; note that $\underline{n}$ is called $\underline{p}$ there). Since in $\mathbb{R}^2$ the direction of a vector is uniquely given by a non-zero normal vector, it suffices to show that the direction of each of the directional derivatives in (5.1) is orthogonal to $\underline{n}$. In symbols, we have to show that

$$\underline{\underline{l}}_{\underline{n}}^{k} \sum_{s=1}^{d} (\partial_{n_s} \lambda_{\underline{n}}^{k} \cdot \underline{\underline{\mathbf{1}}} - \underline{\underline{\boldsymbol{A}}}_s) n_s \stackrel{!}{=} \underline{0}.$$

But we get

$$\underline{\underline{l}}_{\underline{n}}^{k} \sum_{s=1}^{d} (\partial_{n_s} \lambda_{\underline{n}}^{k} \cdot \underline{\underline{\mathbf{1}}} - \underline{\underline{\boldsymbol{A}}}_s) n_s = \underline{\underline{l}}_{\underline{n}}^{k} \sum_{s=1}^{d} \partial_{n_s} \lambda_{\underline{n}}^{k} n_s \cdot \underline{\underline{\mathbf{1}}} - \underline{\underline{l}}_{\underline{n}}^{k} \sum_{s=1}^{d} \underline{\underline{\boldsymbol{A}}}_s n_s = \underline{\underline{l}}_{\underline{n}}^{k} (\underline{n} \cdot \nabla_{\underline{n}} \lambda_{\underline{n}}^{k} - \lambda_{\underline{n}}^{k}).$$

Again using the characteristic theory, we see that this in fact vanishes since $\underline{n} \cdot \nabla_{\underline{n}} \lambda_{\underline{n}}^{k} = \lambda_{\underline{n}}^{k}$, see [14, Lemma 3.4.3]. Thus, we have proven that the integral in the second part of the evolution operator (3.2) can always (except in singular cases, see below) be transformed in such a way that the spatial derivatives of $\boldsymbol{U}$ disappear. We have obtained the following result:

Lemma 5.1. *In the second part of the evolution operator (3.2), the direction of the directional derivative of each component of U is always tangential to the integration path, as long as the parameterization by θ does not become singular.*

We will now demonstrate how this transformation can actually be found. The result of the preceding paragraph is that the direction of the directional derivative of each component of $\boldsymbol{U}$ in (5.1) is tangential to $\partial_\theta \nabla_{\underline{n}} \lambda_{\underline{n}(\theta)}^{k}$, i.e. there must be a vector $\underline{\underline{v}}_{\underline{n}}^{k}$ such that

$$\underline{\underline{l}}^k_{\underline{n}}(\partial_{n_s}\lambda^k_{\underline{n}}\cdot\underline{\underline{1}}-\underline{\underline{A}}_s)=\underline{\underline{v}}^k_{\underline{n}}\partial_\theta\partial_{n_s}\lambda^k_{\underline{n}},\quad s=1,\ldots,d, \tag{5.3}$$

where $\underline{n}$ is always given by (5.2). Inserting this into (3.2), we get that

$$\int_{S^{d-1}}\boldsymbol{r}^k_{\underline{n}}\underline{\underline{l}}^k_{\underline{n}}\sum_{s=1}^{d}(\partial_{n_s}\lambda^k_{\underline{n}}\cdot\underline{\underline{1}}-\underline{\underline{A}}_s)\partial_{x_s}\boldsymbol{U}(\underline{x}+\sigma\nabla_{\underline{n}}\lambda^k_{\underline{n}},\tau)\mathrm{d}\underline{n} \tag{5.4a}$$

$$=\int_0^{2\pi}\boldsymbol{r}^k_{\underline{n}}\underline{\underline{v}}^k_{\underline{n}}\sum_{s=1}^{d}\partial_\theta\partial_{n_s}\lambda^k_{\underline{n}}\partial_{x_s}\boldsymbol{U}(\underline{x}+\sigma\nabla_{\underline{n}}\lambda^k_{\underline{n}},\tau)\mathrm{d}\theta \tag{5.4b}$$

$$=\int_0^{2\pi}\boldsymbol{r}^k_{\underline{n}}\underline{\underline{v}}^k_{\underline{n}}\Big(\partial_\theta\nabla_{\underline{n}}\lambda^k_{\underline{n}}\cdot\nabla_{\underline{x}}\boldsymbol{U}(\underline{x}+\sigma\nabla_{\underline{n}}\lambda^k_{\underline{n}},\tau)\Big)\mathrm{d}\theta \tag{5.4c}$$

$$=\int_0^{2\pi}\boldsymbol{r}^k_{\underline{n}}\underline{\underline{v}}^k_{\underline{n}}\cdot\frac{1}{\sigma}\frac{\mathrm{d}}{\mathrm{d}\theta}\boldsymbol{U}(\underline{x}+\sigma\nabla_{\underline{n}}\lambda^k_{\underline{n}},\tau)\mathrm{d}\theta \tag{5.4d}$$

$$=-\frac{1}{\sigma}\int_0^{2\pi}\frac{\mathrm{d}}{\mathrm{d}\theta}(\boldsymbol{r}^k_{\underline{n}}\underline{\underline{v}}^k_{\underline{n}})\boldsymbol{U}(\underline{x}+\sigma\nabla_{\underline{n}}\lambda^k_{\underline{n}},\tau)\mathrm{d}\theta, \tag{5.4e}$$

where the last equality is the integration by parts with respect to θ; the boundary terms cancel due to the periodicity of the integrand. Furthermore, from (5.3), it follows that

$$\underline{\underline{v}}^k_{\underline{n}}=\frac{1}{|\partial_\theta\nabla_{\underline{n}}\lambda^k_{\underline{n}}|^2}\underline{\underline{l}}^k_{\underline{n}}\sum_{s=1}^{d}\partial_\theta\partial_{n_s}\lambda^k_{\underline{n}}\cdot(\partial_{n_s}\lambda^k_{\underline{n}}\cdot\underline{\underline{1}}-\underline{\underline{A}}_s). \tag{5.5}$$

We thus have found a transformation of the $\underline{n}$ integral of the evolution operator into a form where no derivatives of the solution $\boldsymbol{U}$ occur and the only derivatives that appear can be determined in advance. However, this transformation cannot be applied in the following two cases:

- If $\sigma = 0$, the transformation is undefined. But, since we approximate the time integral with the rectangle rule, we are only interested in the case $\sigma = t_n - t_{n+1} \neq 0$.
- If $\partial_\theta\nabla_{\underline{n}}\lambda^k_{\underline{n}}=\underline{0}$, the transformation is also undefined. This is in particular the case for those modes whose wave fronts degenerate to points. For these modes, we have that the ray velocity $\nabla_{\underline{n}}\lambda^k_{\underline{n}}$ is independent of $\underline{n}$ (and thus of θ). We have not yet examined whether modes for which the wave front is only locally singular also cause problems. We have here in mind such modes, where $\partial_\theta\nabla_{\underline{n}}\lambda^k_{\underline{n}}=\underline{0}$ at a single point, but $\partial_\theta\nabla_{\underline{n}}\lambda^k_{\underline{n}}$ is not entirely independent of θ, cf. the slow magneto-acoustic waves of the MHD equations.

The actual terms which appear in the transformed integral may become very complicated. We found out that there is also a suitable approximation of the integrand, which is comparatively simple. Recall that we anyway approximate the integral by evaluation of the integrand in a finite number of quadrature points. Let θ_i be these quadrature points with respect to θ, and let

$$\underline{n}_i=\underline{n}(\theta_i)=(\cos\theta_i,\sin\theta_i)\quad\text{and}\quad\underline{q}^k_i=\underline{x}+\sigma\nabla_{\underline{n}}\lambda^k_{\underline{n}_i}$$

be the respective quadrature points with respect to $\underline{n}$ and with respect to $\underline{x}$. By $q^k_{i,s}$, we denote the sth component of the vector $\underline{q}^k_i$. Consider now the integrand in (5.4d) at $\theta=\theta_i$ and approximate the θ derivative by a one-sided difference given by the points θ_i and θ_{i+1}. This yields

$$\frac{1}{\sigma}\boldsymbol{r}^k_{\underline{n}}\underline{\underline{v}}^k_{\underline{n}}\frac{\mathrm{d}}{\mathrm{d}\theta}\boldsymbol{U}(\underline{x}+\sigma\nabla_{\underline{n}}\lambda^k_{\underline{n}})\Big|_{\underline{n}=\underline{n}_i}\approx\frac{1}{\sigma}\boldsymbol{r}^k_{\underline{n}_i}\underline{\underline{v}}^k_{\underline{n}_i}\frac{\boldsymbol{U}(\underline{q}^k_{i+1})-\boldsymbol{U}(\underline{q}^k_i)}{\Delta\theta}. \tag{5.6}$$

If we now insert the representation of $\underline{\underline{v}}_{\underline{n}}^k$ given in (5.5) and approximate all θ derivatives in that representation in the same way as above, we can approximate the right-hand side of (5.6) by

$$\frac{1}{\sigma}\boldsymbol{r}_{\underline{\underline{n}}_i}^k \frac{\sigma^2\Delta\theta^2}{|\underline{q}_{i+1}^k - \underline{q}_i^k|^2}\underline{\underline{l}}_{\underline{\underline{n}}_i}^k \sum_{s=1}^{d} \frac{q_{i+1,s}^k - q_{i,s}^k}{\sigma\Delta\theta}\cdot(\partial_{n_s}\lambda_{\underline{\underline{n}}_i}^k \cdot \underline{\underline{\mathbf{1}}} - \underline{\underline{\boldsymbol{A}}}_s)\frac{\boldsymbol{U}(\underline{q}_{i+1}^k) - \boldsymbol{U}(\underline{q}_i^k)}{\Delta\theta}$$
$$= \boldsymbol{r}_{\underline{\underline{n}}_i}^k \underline{\underline{l}}_{\underline{\underline{n}}_i}^k \sum_{s=1}^{d}(\partial_{n_s}\lambda_{\underline{\underline{n}}_i}^k \cdot \underline{\underline{\mathbf{1}}} - \underline{\underline{\boldsymbol{A}}}_s)\frac{(q_{i+1,s}^k - q_{i,s}^k)(\boldsymbol{U}(\underline{q}_{i+1}^k) - \boldsymbol{U}(\underline{q}_i^k))}{|\underline{q}_{i+1}^k - \underline{q}_i^k|^2}.$$

We have thus found an approximation of the integral which does neither contain any derivatives nor essentially more complicated terms than the original integral. Furthermore, we see that our approximation can formally be obtained by just replacing the derivative

$$\partial_{x_s}\boldsymbol{U}(\underline{q}_i^k) \quad \text{with} \quad \frac{(q_{i+1,s}^k - q_{i,s}^k)(\boldsymbol{U}(\underline{q}_{i+1}^k) - \boldsymbol{U}(\underline{q}_i^k))}{|\underline{q}_{i+1}^k - \underline{q}_i^k|^2}. \tag{5.7}$$

Note, however, that there is no reason why this replacement should be a sensible approximation for each s individually. This is only true for the whole integrand. The same result, of course, holds if one uses backward differences, i.e. one replaces

$$\partial_{x_s}\boldsymbol{U}(\underline{q}_i^k) \quad \text{with} \quad \frac{(q_{i-1,s}^k - q_{i,s}^k)(\boldsymbol{U}(\underline{q}_{i-1}^k) - \boldsymbol{U}(\underline{q}_i^k))}{|\underline{q}_{i-1}^k - \underline{q}_i^k|^2}. \tag{5.8}$$

In order to obtain a symmetric formula we use the average of both approximations.

In fact, the $\boldsymbol{U}$ difference is mainly determined by the slopes of the piecewise bilinear reconstruction. However, the above approximation automatically includes an approximation to the Dirac distribution for the discontinuity of the reconstructed $\boldsymbol{U}$ whenever the integration path crosses a cell interface. Just to keep it clear we would like to note that the use of (5.4e) would principally be possible, but the resulting formulae will be too complicated and we have refrained from this choice. Instead we use approximations (5.7), (5.8), which are based on the same fact that enables also (5.4e), but moreover they have an advantage that the Dirac distribution, which appears when the integration path crosses a cell interface, is automatically included.

5.2.2. Singular wave modes

For the modes with singular wave front, the idea in earlier publications, see, e.g. [19], was to insert the differential equation itself into the respective part of the integral equations. This led to a formula where this wave mode was left out completely in the approximate evolution operator and instead certain components of the result were multiplied by corresponding factors. We now found out that there is a generalization of this idea to arbitrary systems. This technique can be applied to any subset of wave modes, no matter whether they are singular or not. The multiplication of certain components with certain factors generalizes to the multiplication of the result with the inverse of a certain $m \times m$ matrix which in general depends on the linearization state. This matrix may, of course, be more or less difficult to invert; it may be badly conditioned or even singular. For the wave equation system as well as for the shallow water equations, this matrix is a diagonal matrix with constant, non-zero diagonal entries, so that the computation of the inverse is trivial.

We will now demonstrate how this generalization works. Let K and K' be two complementary subsets of the set $\{1,\ldots,m\}$ of wave mode indices. For any $k \in K$ and $\underline{n} \in S^{d-1}$, we insert the equality

$$\int_{t_n}^{t_{n+1}} \sum_{s=1}^{d} (\partial_{n_s} \underline{\lambda}_{\underline{n}}^k \cdot \underline{\underline{\mathbf{1}}} - \underline{\underline{\boldsymbol{A}}}_s) \partial_{x_s} \boldsymbol{U}(\underline{x} + (\tau - t_{n+1}) \nabla_{\underline{n}} \underline{\lambda}_{\underline{n}}^k, \tau) \mathrm{d}\tau$$
$$= \int_{t_n}^{t_{n+1}} \left(\partial_t \boldsymbol{U} + \sum_{s=1}^{d} \partial_{n_s} \underline{\lambda}_{\underline{n}}^k \partial_{x_s} \boldsymbol{U} \right) (\underline{x} + (\tau - t_{n+1}) \nabla_{\underline{n}} \underline{\lambda}_{\underline{n}}^k, \tau) \mathrm{d}\tau$$
$$= \int_{t_n}^{t_{n+1}} \frac{\mathrm{d}}{\mathrm{d}\tau} \boldsymbol{U}(\underline{x} + (\tau - t_{n+1}) \nabla_{\underline{n}} \underline{\lambda}_{\underline{n}}^k, \tau) \mathrm{d}\tau = \boldsymbol{U}(\underline{x}, t_{n+1}) - \boldsymbol{U}(\underline{x} - \Delta t \nabla_{\underline{n}} \underline{\lambda}_{\underline{n}}^k, t_n)$$

into the operator (3.2). Collecting $\boldsymbol{U}(\underline{x}, t_{n+1})$, we get

$$\left(\underline{\underline{\mathbf{1}}} - \frac{1}{|S^{d-1}|} \int_{S^{d-1}} \sum_{k \in K} \boldsymbol{r}_{\underline{n}}^k \underline{\underline{l}}_{\underline{n}}^k \mathrm{d}\underline{n} \right) \boldsymbol{U}(\underline{x}, t_{n+1}) = \frac{1}{|S^{d-1}|} \sum_{k \in K'}^{m} \left(\int_{S^{d-1}} \boldsymbol{r}_{\underline{n}}^k \underline{\underline{l}}_{\underline{n}}^k \boldsymbol{U}(\underline{x} - \Delta t \nabla_{\underline{n}} \underline{\lambda}_{\underline{n}}^k, t_n) \mathrm{d}\underline{n} \right.$$
$$+ \int_{t_n}^{t_{n+1}} \int_{S^{d-1}} \boldsymbol{r}_{\underline{n}}^k \underline{\underline{l}}_{\underline{n}}^k \sum_{s=1}^{d} (\partial_{n_s} \underline{\lambda}_{\underline{n}}^k \cdot \underline{\underline{\mathbf{1}}} - \underline{\underline{\boldsymbol{A}}}_s) \partial_{x_s} \boldsymbol{U}(\underline{x} + (\tau - t_{n+1})$$
$$\left. \times \nabla_{\underline{n}} \underline{\lambda}_{\underline{n}}^k, \tau) \mathrm{d}\underline{n} \mathrm{d}\tau \right).$$

Thus, we leave out completely the modes contained in K and then multiply the result of the evolution operator with the inverse of the matrix

$$\underline{\underline{\boldsymbol{J}}}(K) := \underline{\underline{\mathbf{1}}} - \frac{1}{|S^{d-1}|} \int_{S^{d-1}} \sum_{k \in K} \boldsymbol{r}_{\underline{n}}^k \underline{\underline{l}}_{\underline{n}}^k \mathrm{d}\underline{n} = \frac{1}{|S^{d-1}|} \int_{S^{d-1}} \sum_{k \in K'} \boldsymbol{r}_{\underline{n}}^k \underline{\underline{l}}_{\underline{n}}^k \mathrm{d}\underline{n}.$$

As already mentioned, we can choose K to be any subset of $\{1, \ldots, m\}$. However, the more modes we include in K, the more likely the matrix $\underline{\underline{\boldsymbol{J}}}(K)$ might become difficult to invert or even singular. In particular, note that for $K = \{1, \ldots, m\}$, we have $\underline{\underline{\boldsymbol{J}}}(K) = \underline{\underline{\mathbf{0}}}$. Since we have already found a satisfying way to approximate the evolution operator for the non-singular wave modes, cf. Section 5.2.1, we will restrict ourselves to the case that K consists of singular modes.

For example, for the shallow water equations, cf. Lukáčová [18], we have only one singular wave mode, the so-called shear wave mode corresponding to the middle bicharacteristic curve, which points out just the advection direction. If we choose K to consist of this one mode, we get

$$\underline{\underline{\boldsymbol{J}}}(K) = \begin{pmatrix} 1 & 0 & 0 \\ 0 & \frac{1}{2} & 0 \\ 0 & 0 & \frac{1}{2} \end{pmatrix},$$

which can be inverted easily.

For the SMHD equations we have three singular wave modes: the two Alfvén modes (1 and 2) and the non-physical mode (5). For $K = \{1, 2\}$, we get

$$\underline{\underline{\boldsymbol{J}}}(K) = \begin{pmatrix} 1 & 0 & 0 & 0 & 0 \\ 0 & \frac{1}{2} & 0 & 0 & 0 \\ 0 & 0 & \frac{1}{2} & 0 & 0 \\ 0 & 0 & 0 & \frac{1}{2} & 0 \\ 0 & 0 & 0 & 0 & \frac{1}{2} \end{pmatrix}, \tag{5.9}$$

which is comparably easy to handle, but we still have to deal with the non-physical mode. If, on the other hand, we choose $K = \{1, 2, 5\}$, then we get the essentially more complicated matrix

$$\underline{\underline{\boldsymbol{J}}}(K) = \begin{pmatrix} 1 & 0 & 0 & 0 & 0 \\ 0 & \frac{1}{2} & 0 & 0 & 0 \\ 0 & 0 & \frac{1}{2} & 0 & 0 \\ 0 & 0 & 0 & \frac{1}{2} & 0 \\ 0 & 0 & 0 & 0 & \frac{1}{2} \end{pmatrix} - \frac{1}{2\pi} \int_{S^1} \frac{1}{(\underline{B}\cdot\underline{n})^2 + gh} \begin{pmatrix} (\underline{B}\cdot\underline{n})^2 & 0 & 0 & hn_1(\underline{B}\cdot\underline{n}) & hn_2(\underline{B}\cdot\underline{n}) \\ 0 & 0 & 0 & 0 & 0 \\ 0 & 0 & 0 & 0 & 0 \\ gn_1(\underline{B}\cdot\underline{n}) & 0 & 0 & ghn_1^2 & ghn_1n_2 \\ gn_1(\underline{B}\cdot\underline{n}) & 0 & 0 & ghn_1n_2 & ghn_2^2 \end{pmatrix} \mathrm{d}\underline{n}. \tag{5.10}$$

It is not easy, but possible, to find a closed form for the integrals appearing in (5.10). The second term on the right-hand side of (5.10) is a rank 2 matrix. Therefore, $\underline{\underline{\boldsymbol{J}}}(K)$ can be written as the sum of a diagonal matrix and a rank 2 matrix. The Sherman–Morrison–Woodbury formula (see, for example [12, p. 51]) enables us to obtain a comparatively simple representation of the inverse of this matrix. A problem occurs when $\hat{\underline{B}}$ (i.e. the magnetic field of the linearization state) is near zero, because at $\hat{\underline{B}} = \underline{0}$ the matrix $\underline{\underline{\boldsymbol{J}}}(K)$ becomes singular. This means that the choice $K = \{1,2,5\}$ is not allowed when $\hat{\underline{B}}$ is near zero.

Thus, we have the following three main possibilities for replacing the spatial derivatives of $\boldsymbol{U}$ in the case of singular wave modes:

1. Use $K = \{\}$ and approximate the spatial derivatives using the slopes of the piecewise bilinear reconstruction.
2. Use $K = \{1,2\}$ (i.e. use the simple matrix given in (5.9)) and approximate the spatial derivatives for the non-physical mode using the slopes of the piecewise bilinear reconstruction.
3. Use $K = \{1,2,5\}$ (i.e. the more complicated matrix given in (5.10)) if $\hat{\underline{B}}$ is away from zero, but $K = \{1,2\}$ if $\hat{\underline{B}}$ is near zero.

We have experimented numerically with the above three variants. Our numerical results using variants 2 or 3 yield unsatisfactory resolutions, see Section 6.2. Therefore, we suggest to refrain from these possibilities and approximate the spatial derivatives for the singular wave fronts just by using the piecewise bilinear reconstruction. Anyway, note that the problematic case that the spatial integration path crosses a cell interface cannot occur in these cases, since this path reduces to a point.

5.3. Numerical algorithm

1. Given is a piecewise constant approximation at time t_n : $\boldsymbol{U}_{ij}^n$, $i,j \in \mathbb{Z}$, mesh and time steps $\hbar, \Delta t$.
2. *Recovery step:*
   Construct piecewise bilinear functions and apply the limiter procedure, e.g. by using the minmod limter, cf. [21], or monotonized minmod limiter; cf. Section 5.1. This yields the piecewise bilinear approximations $\hat{\psi}^n$, where ψ is an arbitrary component of the vector of primitive variables $(h, \underline{u}, \underline{B})^{\mathrm{T}}$.
3. *Local linearization:*
   At each vertex as well as at each midpoint of cell interfaces choose a linearization state for local linearization, cf. (2.5). This is done by averaging the two or four neighbouring states for a midpoint or a vertex, respectively.
4. *Predictor step/approximate evolution:*
   Compute the intermediate solutions at time level $t_{n+1/2}$ on the cell interfaces by the approximate evolution operators, cf. (3.2) (with Δt replaced with $\Delta t/2$), where $\hat{\boldsymbol{U}}$ is used as the data at t_n. The computation is realized in primitive variables. The approximation of integrals in (3.2) is obtained as follows:
   (a) Integration over S^{d-1} is replaced with finitely many quadrature points of the rectangle rule; cf. Section 5.1.

(b) Time integral, or the so-called mantle integral, in the second part of (3.2) is approximated using the rectangle rule at time t_n.
(c) The spatial derivatives are approximated as explained in Section 5.2.1 (magneto-gravity modes) or by the slopes of $\hat{\boldsymbol{U}}$ (Alfvén and non-physical modes), cf. Section 5.2.2 variant 1. Alternatively, Section 5.2.2, variant 2 and 3 can be used.

5. *Corrector step/FV-update:*
Do the FV-update in conservative variables using the midpoint rule in time and midpoint, trapezoidal or Simpson rule along the cell interfaces. In the experiments presented below we have used the Simpson rule for the flow equations (i.e. first three equations of (4.2)) and the trapezoidal rule for the magnetic field equations (i.e. last two equations of (4.2)). Fluxes at cell interfaces are evaluated at the predicted values obtained by the approximate evolution operator in Step 4.

We remind the reader that the question of suitable quadrature rules along cell interfaces has been extensively studied with respect to stability of the whole FVEG scheme in our previous paper [21]. The use of midpoint rule yields a scheme similar to standard Godunov splitting schemes. By using the combination of the trapezoidal and the Simpson rule we have taken multidimensional effects into account and obtained a scheme, which satisfy the discrete divergence condition, cf. Section 6.3.

6. Numerical examples

We now demonstrate the behavior of the described scheme on test problems for the SMHD equations in one and two space dimensions. We use a CFL number of 0.45 in all computations. We have experimented with different CFL numbers, in fact numerical results indicate that the FVEG scheme stays stable until CFL ≈ 0.56, which is in agreement with stability investigations of the FVEG3 scheme for the linear wave equation system [21,23]. In [20] new quadrature rules for time integration along the bichracteristic cone have been derived and lead to a stability limit close to 1. However, due to a more complex structure of the SMHD system the application of these quadratures is not straightforward and this point should be investigated in future deeply.

6.1. Riemann problem

Our first test example is the Riemann problem used by Rossmanith [31]. It is given by the initial data

$$x < 0: \quad h = 1, \quad \underline{u} = (0,0), \quad \underline{B} = (1,0),$$
$$x > 0: \quad h = 2, \quad \underline{u} = (0,0), \quad \underline{B} = (0.5,1),$$

and the gravitational constant $g = 1$. The numerical solution, that is shown in Fig. 6.1, was computed with a two-dimensional algorithm described above at $t = 0.4$ on the grid with 100 cells in x-direction and 5 cells in y-direction.

The reference solution (solid line) was obtained with the same scheme, but with 1000×5 cells. Comparing the plots with Rossmanith's [31] results, we see that the scheme produces a qualitatively correct solution. We should point out, however, that there are still some oscillations (at both the low and the high resolution) in all components near the right Alfvén discontinuity.

Note that the intrinsic divergence constraint, i.e. $\nabla \cdot (h\underline{B}) = 0$, is automatically maintained, because the flux function F_1 in x_1-direction has got a zero in the component corresponding to the conservative variable hB_1. See also (2.2) and note that the matrix $\underline{B}^{\mathrm{T}}\underline{u} - \underline{u}^{\mathrm{T}}\underline{B}$ has vanishing diagonal entries.

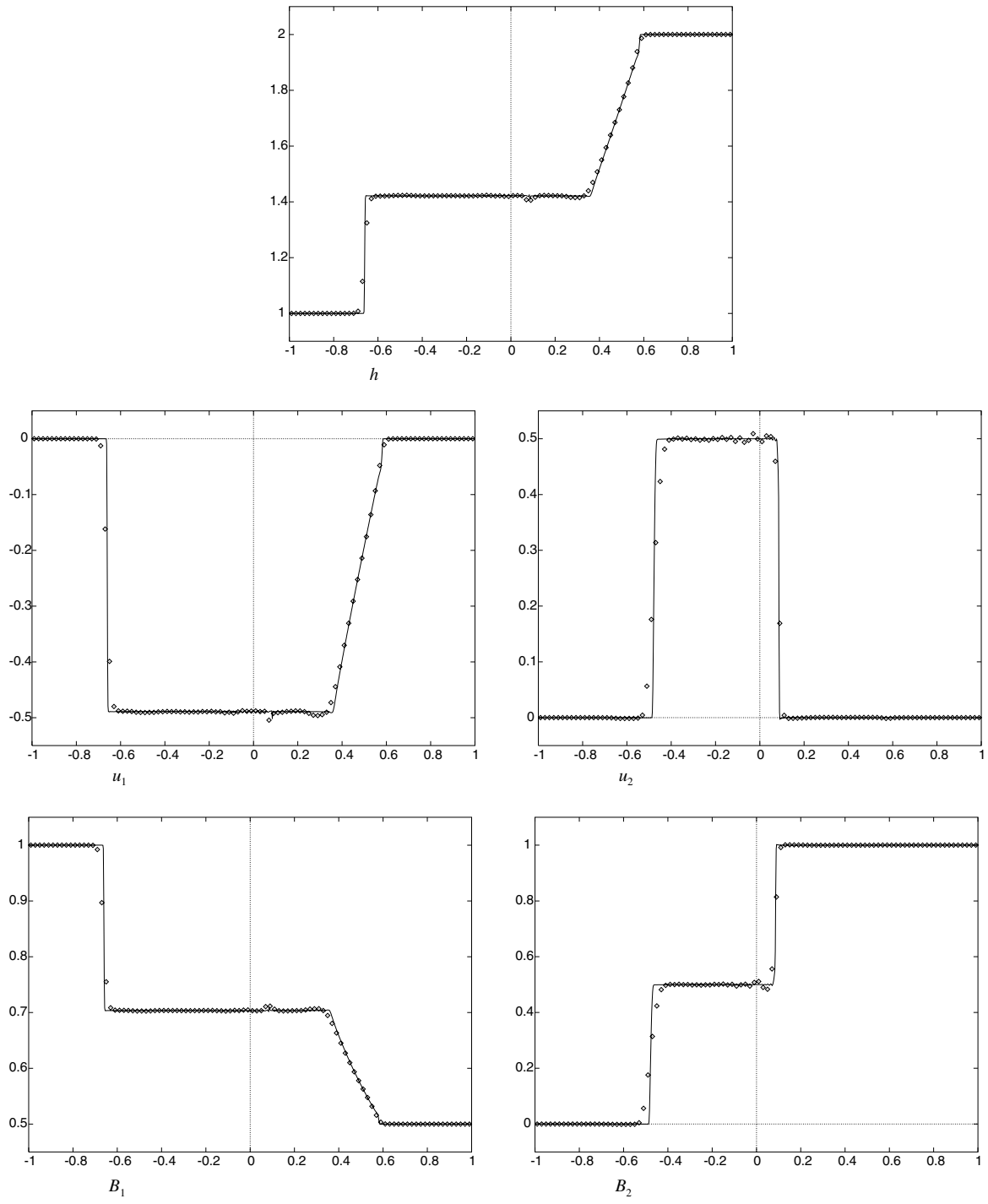

Fig. 6.1. Numerical solution for the Riemann problem with 100×5 cells (dots) and 1000×5 cells (solid line).

6.2. Example for approximations of singular wave modes

We now demonstrate what happens when the singular wave modes are handled by the different approaches proposed in Section 5.2.2. We compute the same one-dimensional Riemann problem as in Section 6.1, but now using the variants 2 and 3, cf. p. 20. The results are shown in Figs. 6.2 and 6.3, respectively.

Both numerical solutions look much worse than the result in Section 6.1, which was computed using the variant 1. We thus suggest to refrain from variants 2 and 3 at all and approximate, as already mentioned in Section 5.2.2, the spatial derivatives for the singular wave modes using the slopes of the piecewise bilinear reconstruction. We think that for these wave modes a better quadrature rule in time (along the bicharacteristic curve), which takes care of possible Dirac distributions for discontinuities of the solution along this curve, could bring better results.

6.3. Two-dimensional problem with shocks

This two-dimensional example is similar to the 'rotor problem' used by Tóth [35] for the MHD equations. The computational domain is $[-1,1]\times[-1,1]$, equipped with zeroth order extrapolation at the boundaries. The initial data are

$$\begin{aligned} \|\underline{x}\| < 0.1: &\quad h = 10, \quad \underline{u} = (-x_2, x_1), \quad \underline{B} = (0.1, 0), \\ \|\underline{x}\| > 0.1: &\quad h = 1, \quad \underline{u} = (0,0), \quad \underline{B} = (1,0), \end{aligned}$$

and the gravitational constant is $g = 1$. Note that $h\underline{B}$ is constant in the initial data and thus divergence-free. The discrete divergence was computed in a vertex-centered way given as

$$\operatorname{div}(h\underline{B})_{i+1/2,j+1/2} = \mu_y \delta_x (hB_1)_{i+1/2,j+1/2} + \mu_x \delta_y (hB_2)_{i+1/2,j+1/2}, \quad i,j \in \mathbb{Z}, \tag{6.1}$$

where $\psi_{i\pm1/2,j\pm1/2} := \psi((i \pm 1/2)\hbar, (j \pm 1/2)\hbar)$ denotes the values of any function ψ at vertices of the mesh cell K_{ij}. Here we used the finite difference operators

$$\mu_x \psi(x) = \frac{1}{2}[\psi(x + \hbar/2) + \psi(x - \hbar/2)], \quad \delta_x \psi(x) = \psi(x + \hbar/2) - \psi(x - \hbar/2)$$

with an analogous notation for the y-direction. In fact the particular choice of the trapezoidal rule for the flux interface integrals of the Maxwell equations yields such a structure of the FVEG scheme which fulfills also more general conditions needed in order to satisfy the divergence-free constraint in general [33]. We should also point out that in [24] the discrete vorticity for the wave equation system was defined in an analogous way to (6.1). It has been shown in [24] that the Lax–Wendroff (Richtmyer rotated) scheme is vorticity-preserving. Actually, the multidimensional FVEG scheme that uses the trapezoidal rule for cell interfaces shares some similarities with the Lax–Wendroff scheme.

In the following we will show that for the numerical solution of the FVEG scheme the discrete divergence defined in (6.1) is constant in time, more precisely we show that if it was zero initially, it stays zero at any time. Consider the last two equations of (2.1) and (2.2), i.e. the Maxwell equations

$$\partial_t \begin{pmatrix} hB_1 \\ hB_2 \end{pmatrix} + \partial_x \begin{pmatrix} 0 \\ -f \end{pmatrix} + \partial_y \begin{pmatrix} f \\ 0 \end{pmatrix} = \begin{pmatrix} 0 \\ 0 \end{pmatrix},$$

where $f = hB_1u_2 - hB_2u_1$ is the flux function. Further let us denote by $f_{i\pm1/2,j}$ and $f_{i,j\pm1/2}$ the approximations of the fluxes at cell interfaces, which are obtained by the trapezoidal rule using the intermediate solution U^* at vertices. Thus, we have, for example for the right and upper cell interfaces,

$$f_{i+1/2,j} = \mu_y f(\boldsymbol{U}^*_{i+1/2,j}), \quad f_{i,j+1/2} = \mu_x f(\boldsymbol{U}^*_{i,j+1/2}).$$

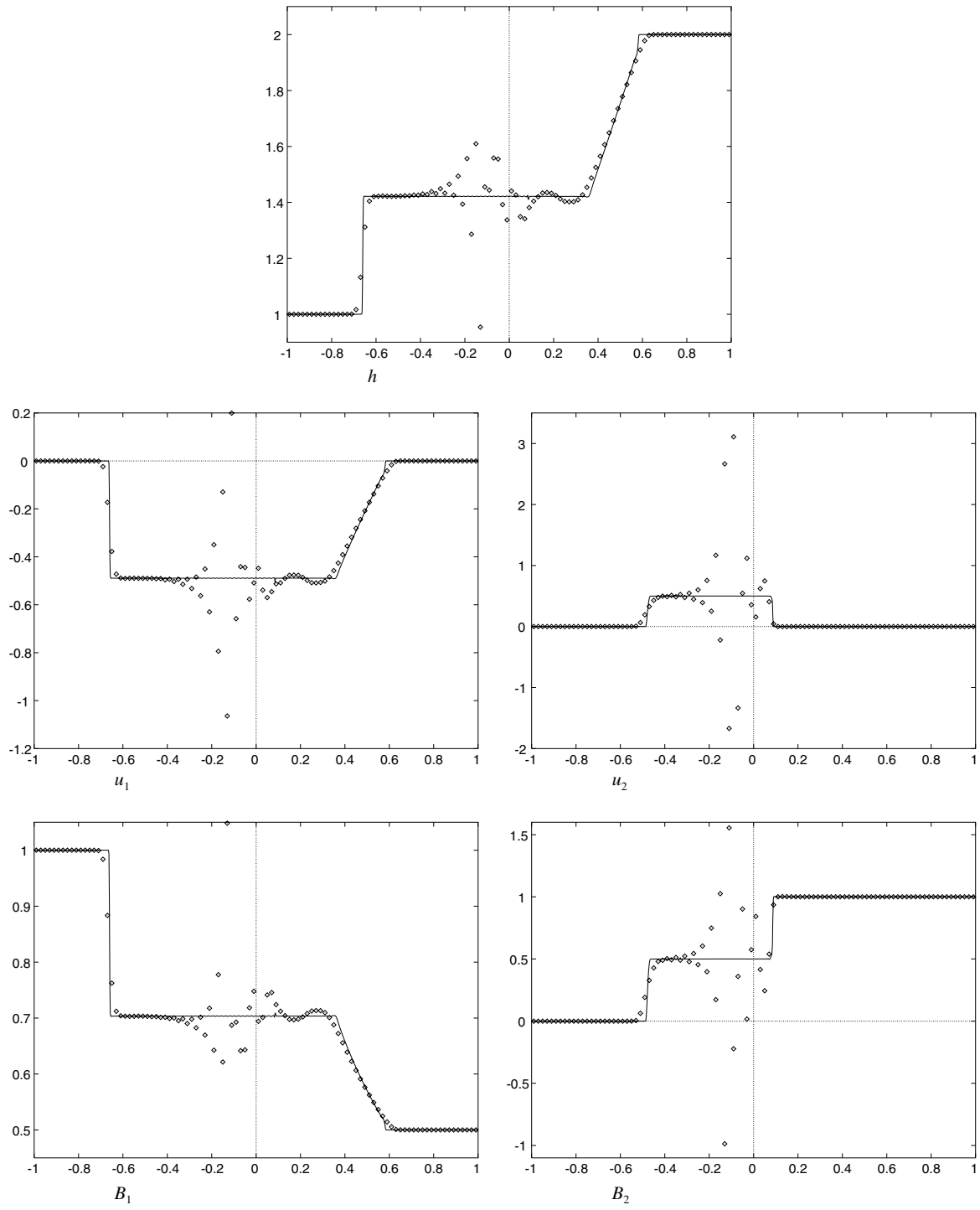

Fig. 6.2. Numerical solution for the Riemann problem with 100×5 cells using variant 2 of Section 6.1.

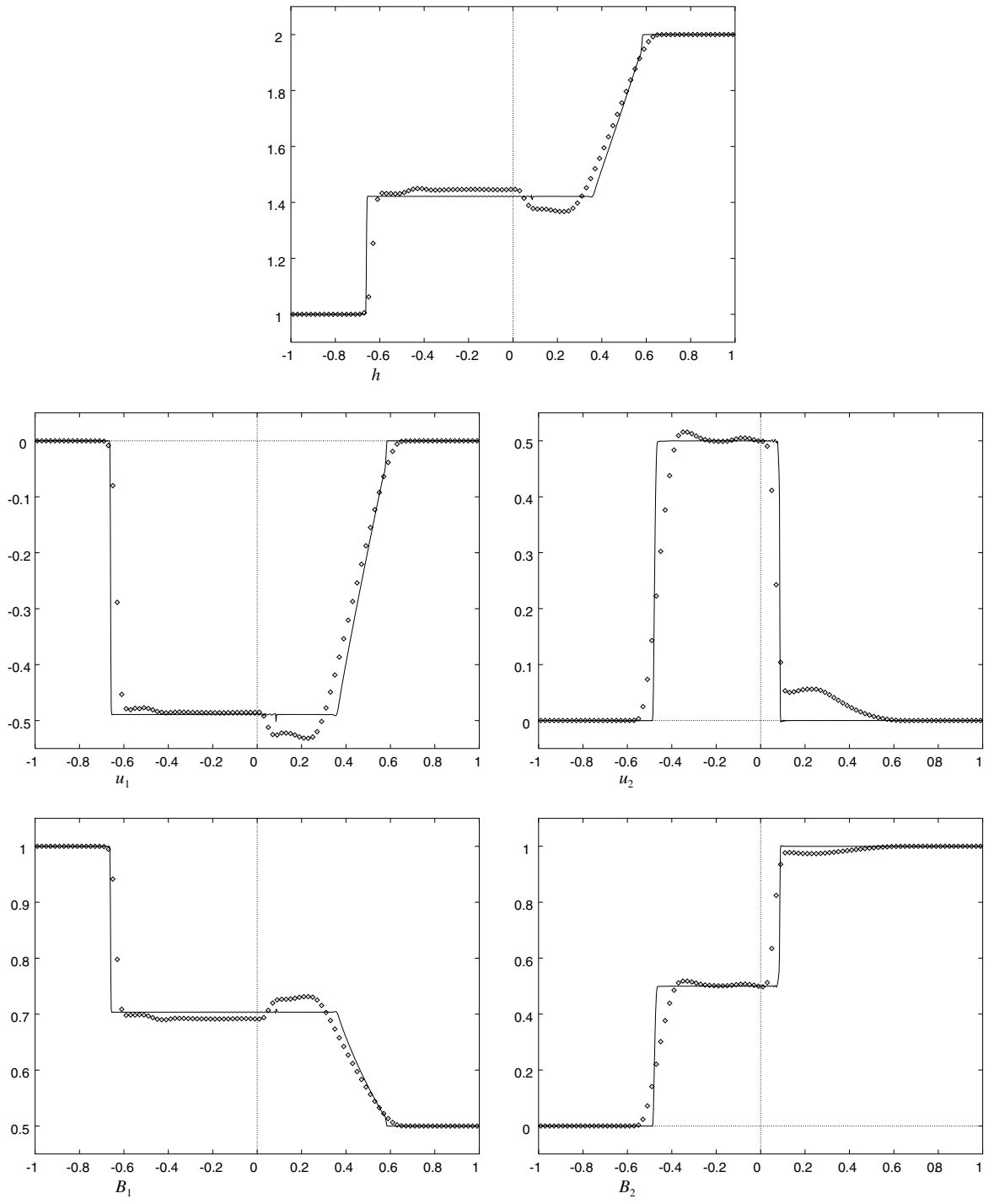

Fig. 6.3. Numerical solution for the Riemann problem with 100×5 cells using variant 3 of Section 6.1.

The intermediate approximations at vertices U^* are obtained by the approximate evolution operator, i.e. using approximation of the evolution operator (3.1) at each vertex.

Now assume that at time t_n, $\mathrm{div}(h\underline{B})^n_{i+1/2,j+1/2} = 0,\ i,j \in \mathbb{Z}$. Then it follows from the FV update as well as from (6.1) that

$$\mathrm{div}(h\underline{B})^{n+1}_{i+1/2,j+1/2} = -\frac{\Delta t}{\hbar}\left[\mu_y\delta_x\delta_y\mu_x f(\boldsymbol{U}^*_{i+1/2,j+1/2}) - \mu_x\delta_y\delta_x\mu_y f(\boldsymbol{U}^*_{i+1/2,j+1/2})\right] = 0. \tag{6.2}$$

Our numerical experiments confirm that the discrete divergence (6.1) is zero up to the machine precision for different mesh parameters $\hbar$.

Contour plots of the result at $t = 0.2$ for 200×200 cells are shown in Fig. 6.4. Plots with higher resolution, i.e. 300×300 cells, are shown in Fig. 6.5. We can notice that the FVEG scheme resolves correctly multidimensional discontinuities as expected.

6.4. Empirical order of convergence

In this experiment we test experimental order of convergence for a smooth solution. We consider the initial value problem for two-dimensional SMHD equation with the initial values

$$h(\underline{x},0) = \frac{1}{4},\ B_1(\underline{x},0) = \frac{1}{2},\ B_2(\underline{x},0) = 1,$$

$$u(\underline{x},0) = 1 + \frac{1}{2}\sin(\pi y) + \frac{1}{4}\cos(\pi x),$$

$$v(\underline{x},0) = 1 + \frac{1}{4}\sin(\pi x) + \frac{1}{2}\cos(\pi y);$$

see also [34] for an analogous test problem for the full MHD system. Although an exact solution is not known, we can still study the experimental order of convergence (EOC). This is computed in the following way using three meshes of sizes N_1, $N_2 := N_1/2$, $N_3 := N_2/2$, respectively,

$$\mathrm{EOC} = \log_2 \frac{\|\boldsymbol{U}^n_{N_2} - \boldsymbol{U}^n_{N_3}\|}{\|\boldsymbol{U}^n_{N_1} - \boldsymbol{U}^n_{N_2}\|}.$$

Here, $\boldsymbol{U}^n_N$ is the approximate solution on the mesh with $N \times N$ cells. The computational domain $[-1,1]\times[-1,1]$ was consecutively divided into $20\times 20, 40\times 40, \ldots, 160\times 160$ cells. The final time was taken to be $t = 0.2$. Table 1 and Table 2 show the experimental order of convergence computed in the L^2 and L^1 norms, respectively. We also show the convergence rate for the first component h as well as for the magnetic field $\underline{B}$. It can be seen clearly that the experimental order of convergence is 2. Note, however, a slightly decreasing order of the convergance rate on finer meshes. We believe that a more suitable quadrature rules for time integrals in the second part of the integral equations (3.2), which would be analogous to those of the Euler equations [20], will increase a stability range of the scheme as well as its global accuracy. To do this it would be necessary to derive an approximate evolution operator without spatial derivatives of unknown function. This is a point for future study.

6.5. Two-dimensional explosion problem/transcritical flow

This is a two-dimensional analogy of the cylindrical explosion problem for the gas dynamics, cf. the Sod 2D problem [20]. The initial data are

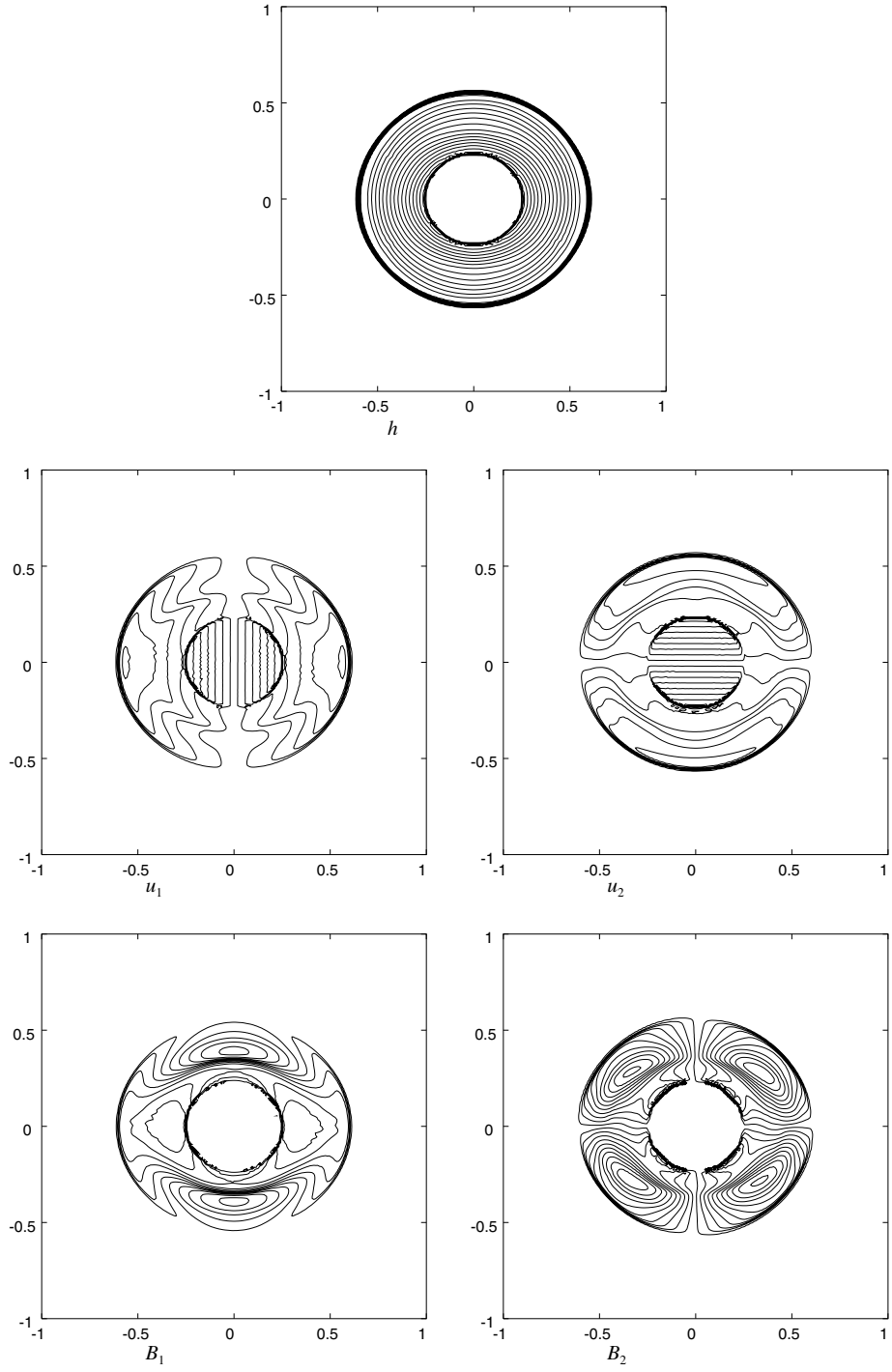

Fig. 6.4. Contour plots of the two-dimensional rotor-like problem with 200×200 cells.

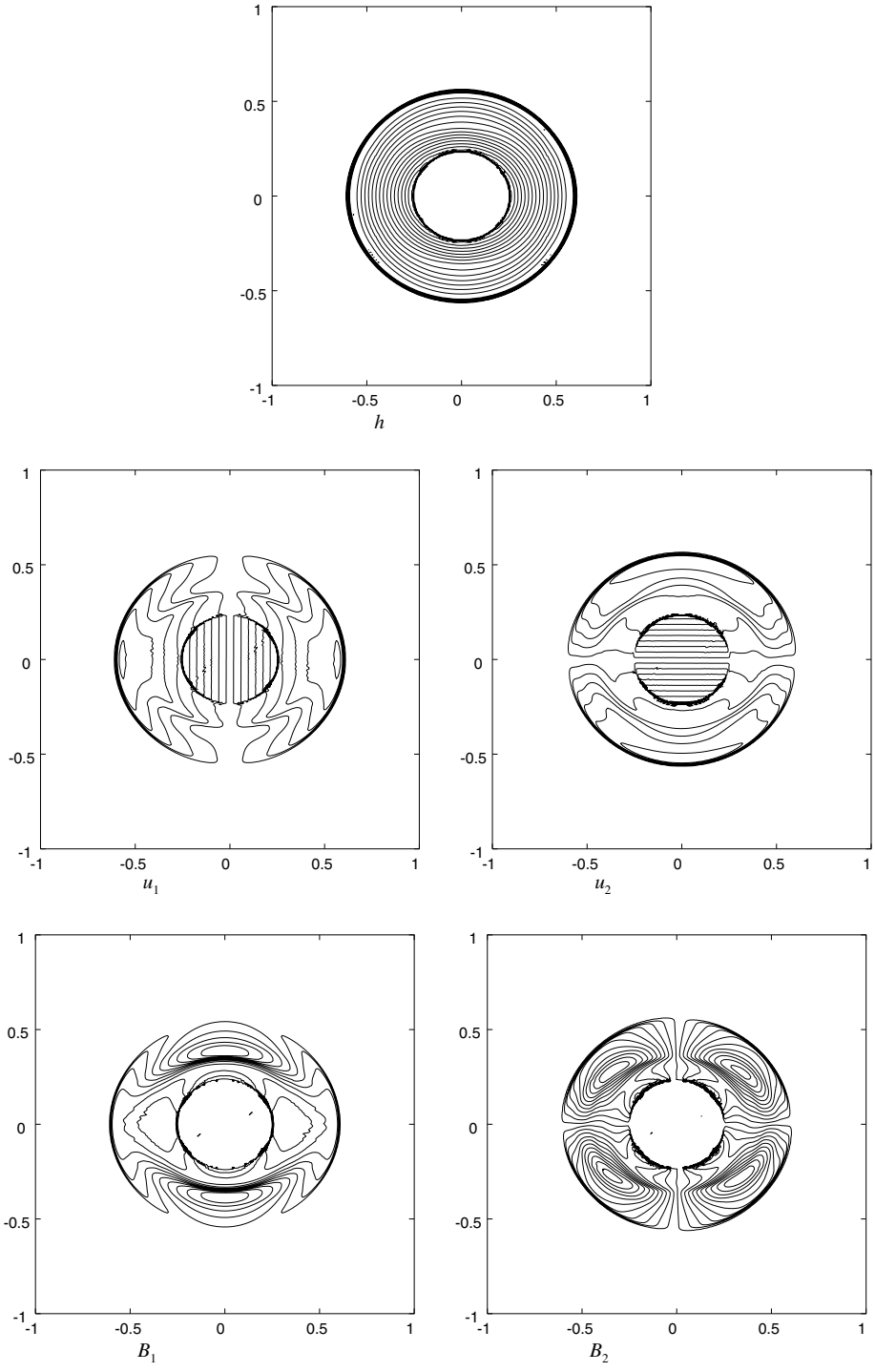

Fig. 6.5. Contour plots of the two-dimensional rotor-like problem with 300×300 cells.

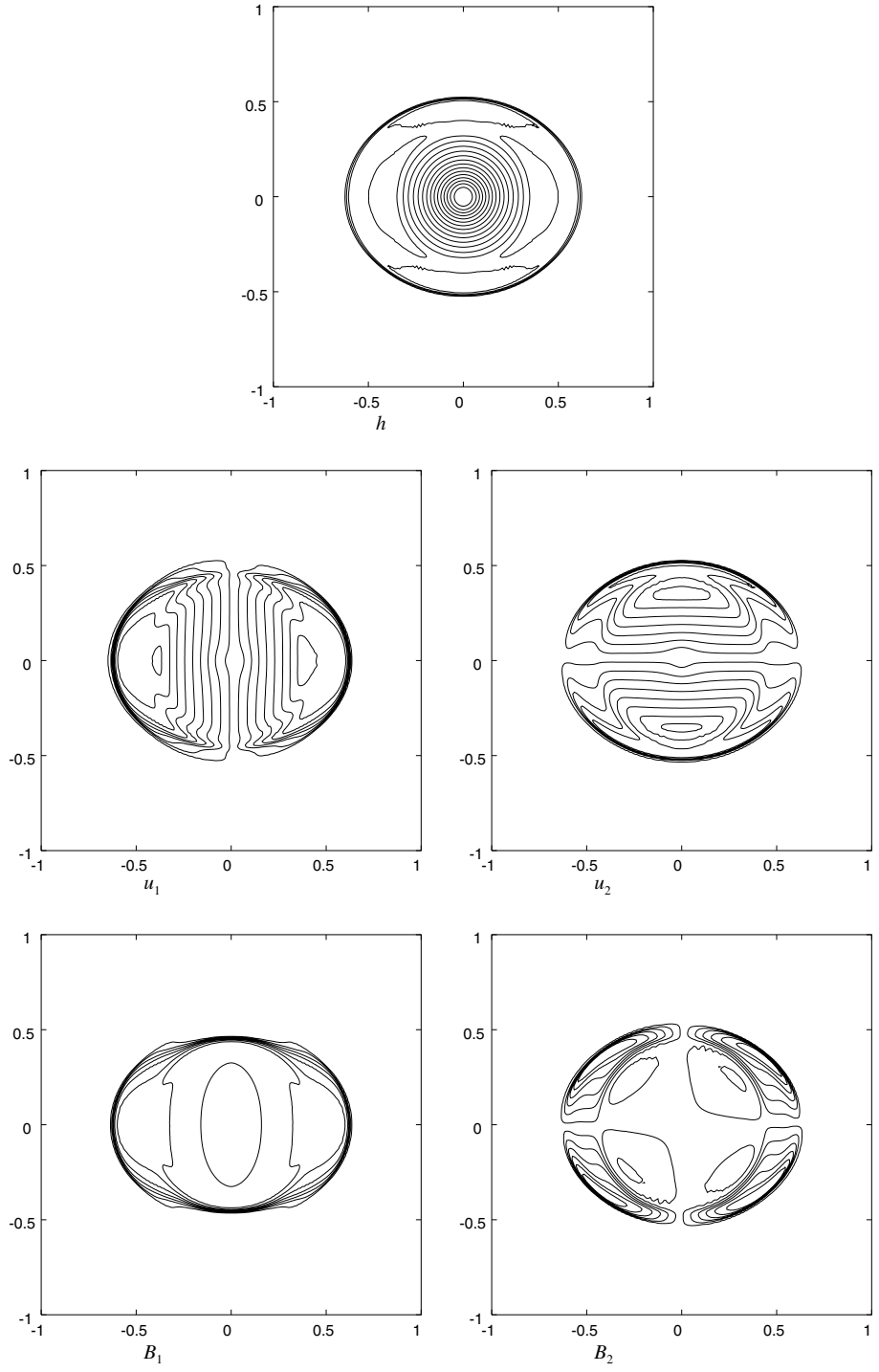

Fig. 6.6. Contour plots of the two-dimensional explosion problem with 200×200 cells.

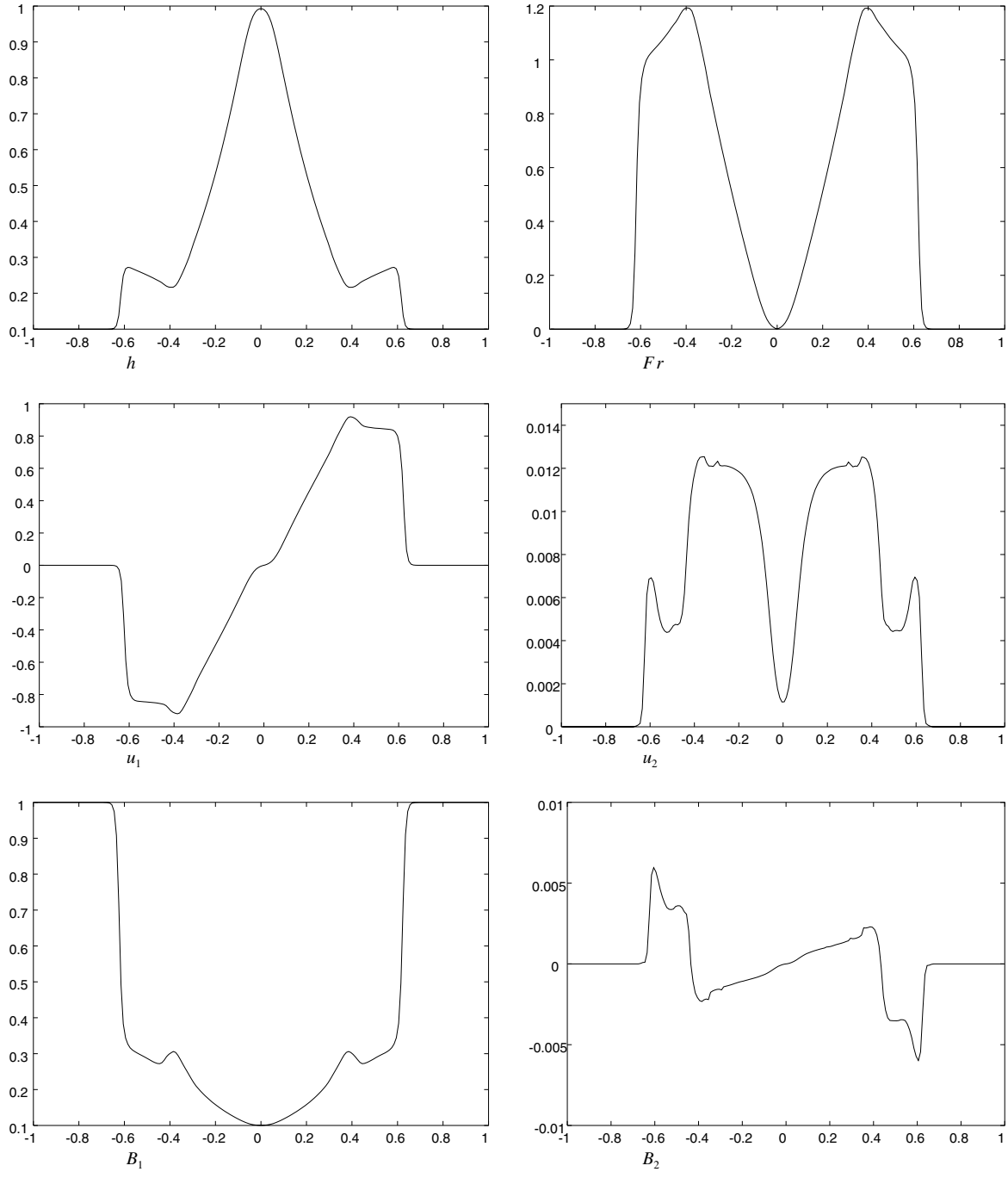

Fig. 6.7. Graph of the solution of the two-dimensional explosion problem with 200×200 cells, cross-section for $y = 0$.

$$h = 1, \quad u_1 = 0, \quad u_2 = 0, \quad B_1 = 1, \quad B_2 = 0, \quad \|\underline{x}\| < 0.3,$$
$$h = 0.1, \quad u_1 = 0, \quad u_2 = 0, \quad B_1 = 0.1, \quad B_2 = 0 \quad \text{else}.$$

In an analogy to the Sod problem for gas dynamics, the flow is transcritical, i.e. $Fr := \sqrt{u_1^2 + u_2^2}/\sqrt{gh + B_1^2 + B_2^2}$ is larger, equal or smaller than 1, cf. Fig. 6.7. It should be pointed out that the FVEG method needs no special entropy fix correction in order to resolve correctly critical states, i.e. $Fr = 1$. This is again analogous to the situation of the Euler equations, see also [21].

The computational domain is a square $[-1,1]\times[-1,1]$, the mesh is rectangular and the initial data are implemented by cutting the initial discontinuity and assigning it by modified area-weighted values according to the corresponding cell. The initial data are moreover discretized in such a way that diveregence of $h\,\underline{B}$ stays zero. Fig. 6.6 shows the isolines of height and x,y-components of velocity, magnetic field and the parameter Fr computed at time $t = 0.25$. It can be seen clearly that due to the influence of the magnetic field the solution is now no more rotationally symmetric as it was the case of the Sod 2D problem for the gas dynamics. The solution exhibits a shock traveling away from the center, a rarefaction wave traveling towards the origin at $(0,0)$ and two Alfvén waves. In Fig. 6.7 the $y = 0$ cross-sections are plotted; slower Alfvén waves that are located between the rarefaction wave and the shock are evident in the tangential components of velocity and magnetic field. Small oscillations near the Alfvén modes can be noticed, however we should also take into account that the scalling of u_2 and B_2 graphs is of order 10^{-3}. The discrete divergence (6.1) stays zero up to the machine accuracy.

We mention that an analogous initial data problem have been studied extensively by many authors for the full ideal MHD system, see, e.g. [2]. Since the MHD system is a non-convex, non-strictly hyperbolic system, there exist discontinuities that are evolutionary and non-evolutionary. If a strictly coplanar problem (2D problem) for the MHD system is considered the solution can be non-unique. Depending on a scheme a non-evolutionary solution in the form of the so-called compound wave can be found. In fact, this compound wave is unstable, under normal perturbations in transverse quantities it is changed into a rotational discontinuity and a slow shock, cf., e.g. [16]. For the SMHD system it is important to realize that $\nabla\lambda_k \mathbf{r}^k$, $k = 3,4$, do not change sign. Thus, the magneto-gravity modes are convex and we do not have compound shocks.

7. Conclusion

In the present paper we have derived a second-order FVEG scheme for the SMHD equations. Up to our knowledge, this is the first attempt to apply genuinely multidimensional EG technique to a magnetohydrodynamic model. We have derived an integral equations for the SMHD equations, cf. (3.2), and discussed its suitable approximation. We have studied more deeply the approximation of the spatial derivatives in the integral equations (3.2) for singular as well as non-singular wave modes. More precisely, we have shown that for arbitrary hyperbolic conservation laws, the spatial derivatives of the solution $\boldsymbol{U}$ can be replaced by means of the Gauss theorem with the derivatives of the eigenvectors themselves, cf. Lemmas 5.1 and 5.4.

Due to the complex eigenstructure which arises in the SMHD system, it is still rather complicated to apply this result directly. Instead we propose to exploit this result numerically as given in (5.6). Our numerical experiments confirm the reliability of this approach for non-singular wave modes.

Treatment of the singular wave modes is more delicate. Our numerical experiments show that the approximation of the derivatives in (3.2) by slopes of the bilinear reconstruction yields the best results, cf. Section 6.2. We believe that more suitable numerical quadratures for the mantle integrals from t_n to t_{n+1} in the integral equations (3.2) can increase accuracy as well as stability of the scheme. They should, analogously as in [20], reflect propagation of one-dimensional waves exactly. This is a subject of our future study.

Table 1
FVEG scheme/convergence in the L^2 norm

N	$\|\boldsymbol{U}^n_{N/2} - \boldsymbol{U}^n_N\|$	EOC	$\|h^n_{N/2} - h^n_N\|$	EOC	$\|\underline{B}^n_{N/2} - \underline{B}^n_N\|$	EOC
20	0.007317		0.002130		0.003234	
40	0.001721	2.0880	0.000501	2.0879	0.000793	2.0279
80	0.000406	2.0837	0.000116	2.1107	0.000204	1.9588
160	0.000107	1.9239	0.000034	1.7705	0.000056	1.8651

Table 2
FVEG scheme/convergence in the L^1 norm

N	$\|\boldsymbol{U}^n_{N/2} - \boldsymbol{U}^n_N\|$	EOC	$\|h^n_{N/2} - h^n_N\|$	EOC	$\|\underline{B}^n_{N/2} - \underline{B}^n_N\|$	EOC
20	0.011766		0.001508		0.002569	
40	0.002837	2.0522	0.000344	2.1322	0.000647	1.9894
80	0.000702	2.0148	0.000080	2.1043	0.000172	1.9114
160	0.000187	1.9084	0.000024	1.7370	0.000047	1.8716

The discretization of the flux interface integrals for the magnetic field, i.e. for the Maxwell equations part, was done by the trapezoidal rule. In such a way the discrete divergence (6.1) is identically zero at each vertex.

One major advantage of the current description and implementation of the FVEG scheme is that it is designed in a black-box like manner and should therefore be applicable to any system of hyperbolic conservation laws with comparatively low effort, if the complete hyperbolic structure of the system is known (see Tables 1 and 2).

Acknowledgments

This research has been supported by the Graduate College 'Conservation principles in the modelling and simulation of marine, atmospherical and technical systems' of Deutsche Forschungsgemeinschaft. We would like to thank Prof. E. Tadmor, University of Maryland, College Park, for a fruitful discussion on the div-free condition. We also want to thank Prof. H. Voß, TU-Hamburg-Harburg, for supporting our work.

References

[1] J.U. Brackbill, D.C. Barnes, The effect of nonzero $\nabla \cdot B$ on the numerical solution of the magnetohydrodynamic equations, J. Comput. Phys. 35 (1980) 426–430.
[2] M. Brio, C.C. Wu, An upwind differencing scheme for the equations of ideal magnetohydrodynamics, J. Comput. Phys. 75 (1988) 400–422.
[3] M. Brio, A.R. Zakharian, G.M. Webb, Two-dimensional Riemann solver for Euler equations of gas dynamics, J. Comput. Phys. 167 (1) (2001) 177–195.
[4] D.S. Butler, The numerical solution of hyperbolic systems of partial differential equations in three independent variables, Proc. Roy. Soc. London, Ser. A 255 (1960) 232–252.
[5] R. Courant, D. Hilbert, Methods of Mathematical Physics. Partial Differential Equations, vol. II, Interscience, New York, 1962.
[6] H. DeSterck, Hyperbolic theory of the "shallow water" magnetohydrodynamics equations, Phys. Plasmas 8 (7) (2001) 3293–3304.
[7] M. Fey, Multidimensional upwinding. I. The method of transport for solving the Euler equations, J. Comput. Phys. 143 (1998) 159–180.

[8] M. Fey, Multidimensional upwinding. II. Decomposition of the Euler equations into advection equations, J. Comput. Phys. 143 (1998) 181–199.
[9] P.A. Gilman, Magnetohydrodynamic "shallo water" equations for the solar tachocline, Astrophys. J. Lett. 544 (2000) L79–L82.
[10] S.K. Godunov, A difference scheme for numerical computation of discontinuous solutions of equations of fluid dynamics, Mat. Sb. 47 (1959) 271–306.
[11] S.K. Godunov, Symmetric form of the equations of magnetohydrodynamics, Numer. Method Mech. Cont. Med. 1 (1972) 26–34.
[12] G.H. Golub, C.F. van Loan, Matrix Computations, third ed., Johns Hopkins Univ. Press, Baltimore, 1996.
[13] A. Jeffrey, T. Taniuti, Non-Linear Wave Propagation, Academic Press, New York, 1964.
[14] T. Kröger, Multidimensional systems of hyperbolic conservation laws, numerical schemes, and characteristic theory – connections, differences, and numerical comparison, Dissertation, Aachen, 2004.
[15] T. Kröger, S. Noelle, S. Zimmermann, On the connection between some Riemann-solver free approaches to the approximation of multi-dimensional systems of hyperbolic conservation laws, M^2AN 38 (6) (2004) 989–1009.
[16] A.G. Kulikovskii, N.V. Pogorelov, A.Yu. Semenov, Mathematical Aspects of Numerical Solution of Hyperbolic Systems, Monograph and Surveys in Pure and Applied Mathematics, Chapman & Hall/CRC Press, Englewood Cliffs, NJ/Boca Raton, FL, 2001.
[17] R.J. LeVeque, Wave propagation algorithms for multidimensional hyperbolic systems, J. Comput. Phys. 131 (2) (1997) 327–353.
[18] M. Lukáčová-Medvid'ová, Multidimensional bicharacteristic finite volume methods for the shallow water equations, in: R. Herbin, D. Kröner (Eds.), Finite Volumes for Complex Applications, Hermes, 2002, pp. 389–397.
[19] M. Lukáčová-Medvid'ová, K.W. Morton, G. Warnecke, Evolution Galerkin methods for hyperbolic systems in two space dimensions, Math. Comput. 69 (2000) 1355–1384.
[20] M. Lukáčová-Medvid'ová, K.W. Morton, G. Warnecke, Finite volume evolution Galerkin (FVEG) methods for hyperbolic sytems, SIAM J. Sci. Comput. 26 (1) (2004) 1–30.
[21] M. Lukáčová-Medvid'ová, J. Saibertová, G. Warnecke, Finite volume evolution Galerkin methods for nonlinear hyperbolic sytems, J. Comput. Phys. 183 (2) (2002) 533–562.
[22] M. Lukáčová-Medvid'ová, G. Warnecke, Y. Zahaykah, Third order finite volume evolution Galerkin (FVEG) methods for two-dimensional wave equation system, J. Numer. Math. 11 (3) (2003) 235–251.
[23] M. Lukáčová-Medvid'ová, G. Warnecke, Y. Zahaykah, On the stability of the evolution Galerkin schemes applied to a two-dimensional wave equation system (submitted).
[24] K.W. Morton, P.L. Roe, Vorticity-preserving Lax–Wendroff-type schemes for the system wave equation, SIAM J. Sci. Comput. 23 (1) (2001) 170–192.
[25] S. Noelle, The MoT-ICE: a new high-resolution wave-propagation algorithm for multidimensional systems of conservation laws based on Fey's method of transport, J. Comput. Phys. 164 (2) (2000) 283–334.
[26] S. Ostkamp, Multidimensional characteristic Galerkin schemes and evolution operators for hyperbolic systems, Dissertation, Hannover, 1995.
[27] S. Ostkamp, Multidimensional characteristic Galerkin methods for hyperbolic systems, Math. Meth. Appl. Sci. 20 (13) (1997) 1111–1125.
[28] K.G. Powell, An approximate Riemann solver for magnetohydrodynamics (that works in more than one dimension), ICASE-Report 94 24 (NASA CR 194902), 1994.
[29] P. Prasad, Nonlinear Hyperbolic Waves in Multi-dimensions, Chapman & Hall/CRC Press, New York/Boca Raton, FL, 2001.
[30] P.L. Roe, Discrete models for the numerical analysis of time-dependent multidimensional gas dynamics, J. Comput. Phys. 63 (1986) 458–476.
[31] J.A. Rossmanith, A Wave Propagation Mathod with Constrained Transport for Ideal and Shallow Water Magnetohydrodynamics, Dissertation, Washington, 2002.
[32] P.K. Sweby, High resolution schemes using flux limiters for hyperbolic conservation laws, SIAM J. Numer. Anal. 21 (2) (1984) 995–1011.
[33] E. Tadmor, Private communication, Oberwolfach, 2004.
[34] M. Torrilhon, Zur Numerik der Idealen magnetohydrodynamik, ETH Dissertation, Zürich, Shaker Verlag, Aachen, 2004.
[35] G. Tóth, The $\nabla \cdot B = 0$ constraint in shock-capturing magnetohydrodynamics codes, J. Comput. Phys. 161 (2) (2000) 605–652.